Chemical Engineering Science 336 (2026) 124502

Contents lists available at ScienceDirect

Chemical Engineering Science

journal homepage: www.elsevier.com/locate/ces

Large eddy simulation of segregating multiphase pipe flows using Lagrangian particle tracking and Eulerian hindered settling models

Md Mahidul Haque Prodhan [a,b,*], Michael Fairweather [a], Jeffrey Peakall [c], Timothy N. Hunter [a,*]

[a] *School of Chemical and Process Engineering, University of Leeds, Leeds LS2 9JT, United Kingdom*
[b] *Department of Nuclear Engineering, University of Dhaka, Dhaka 1000, Bangladesh*
[c] *School of Earth and Environment, University of Leeds, Leeds LS2 9JT, United Kingdom*

ARTICLE INFO

Keywords:
Large eddy simulation (LES)
Lagrangian particle tracking
Eulerian approach
Particle segregation
Hindered settling

ABSTRACT

Evaluating the segregation and settling of particles undergoing hydraulic transport in pipelines is critically important to many industrial installations across sectors such as minerals processing and waste management. Computational fluid dynamics can be used both to aid in their design and identify challenges in operation. To better understand the multiphase flow physics involved in such operations, the primary goal of this research is to simulate the complex particle concentration distribution in transport pipelines using large eddy simulation. This approach is coupled to a validated Lagrangian particle tracking (LPT) method that is compared with an implicit Eulerian-Eulerian (EE) approach to predict flows with low particle volume fractions to confirm the accuracy of the latter model. The EE model is subsequently applied to intermediate and high-volume fraction flows, given the volume fraction limitations of the LPT approach, with both experimental and numerical datasets compared for validation. Finally, a comparison of particle settling predicted using the EE approach coupled to a hindered settling model is compared with predictions obtained without hindered settling. Results highlight the superiority of predictions incorporating hindering, and that for the flows considered, equilibrium profiles are formed over moderate timescales of 60–80 s. In addition, hindered settling significantly reduces particle segregation at concentrations >3 vol%. Overall, the EE hindered settling approach provides a computationally efficient, yet high resolution methodology, for simulation of particulate flows typical of many industrially relevant problems. Ongoing work is employing population balance techniques to simulate flocculation break-up in solid–liquid systems.

1. Introduction

Nuclear energy is a form of low-carbon energy thanks to the minimal CO_2 emissions during its operation, but processing radioactive waste presents a significant challenge that demands expertise in predicting particle transport properties in a variety of slurry processing problems (Cunliffe et al., 2021; Hussain et al., 2022). Particle-laden turbulent flows are also of relevance in numerous other industrial arenas such as chemical engineering, multiphase reactors, wastewater treatment, mineral tailings management and processing of industrial effluents, to name a few (Wu et al., 2024). These applications involve blends of gas and liquid phases (Yan et al., 2024), two immiscible liquids (Li et al., 2023), as well as liquid and solid phases (Benn et al., 2018; Jo et al., 2022). The design and optimisation of such industrial processes rely on a comprehension of system hydrodynamics conventionally obtained through experimental flow loops.

As an alternative, computational fluid dynamics (CFD) is an important tool for simulating the complex multiphase flows in such systems, and can be used where there is a lack of relevant experimental data, specifically for solid–liquid pipe flows (Dixit et al., 2023; Sadeghi et al., 2022; Shajahan et al., 2024; Yang et al., 2022; Zhang et al., 2021; Zheng et al., 2020). However, even though researchers have exploited CFD models effectively in process design, further advances are crucial for a better understanding of industrially-relevant multiphase flows (Lv et al., 2024). CFD offers a cost-effective means of analysing industrial processes (Fazeli et al., 2024), and for multiphase flows, two approaches are generally used in their solution: Eulerian-Eulerian techniques, where both phases are predicted by solving continuum equations, and Eulerian-Lagrangian approaches where the fluid is treated as Eulerian

* Corresponding authors.
E-mail addresses: prodhan@du.ac.bd (M.M.H. Prodhan), t.n.hunter@leeds.ac.uk (T.N. Hunter).

https://doi.org/10.1016/j.ces.2026.124502
Received 10 February 2026; Received in revised form 28 April 2026; Accepted 20 June 2026
Available online 21 June 2026

Nomenclature

Symbols and fundamental equations	Meaning (units)
$\boldsymbol{U}$	Velocity (m/s)
ρ	Density (kg/m^3)
P	Pressure (Pa)
C	Particle concentration (g/L)
$\boldsymbol{F}$	Force (N/m^2)
g	Gravitational acceleration (m/s^2)
μ	Dynamic viscosity (kg/m.s)
ν	Kinematic viscosity (m^2/s)
α	Volume fraction
d	Particle Diameter (m)
D	Pipe diameter (m)
Re	Reynolds number
C_d	Drag coefficient
R_z	Richardson-Zaki constant
$\gamma = \frac{\mu}{\rho}$	Kinematic viscosity (m^2/s)
$\mathrm{Re_b} = \frac{U_b\delta}{\gamma_f} = \frac{\rho_f U_b \delta}{\mu_f}$	Bulk Reynolds number
$\mathrm{Re}_\tau = \frac{U_\tau\delta}{\gamma_f} = \frac{\rho_f U_\tau \delta}{\mu_f}$	Shear Reynolds number
$\delta = \frac{4\times crosssectionalarea}{perimeter}$	Characteristic length
$U_b = \frac{volumetricflowrate}{crosssectionalarea}$	Bulk velocity
$U_\tau = \sqrt{\frac{wallshearstress}{fluiddensity}}$	Shear velocity
$St^+ = \frac{\text{particulate phase relaxation time}}{\text{viscous flow time scale}} = \frac{\tau_p}{\tau_f} = \frac{\left(d_p{}^*\right)^2 \rho_p{}^* Re_\tau{}^2}{18} \tau_p = \frac{\rho_p d_p{}^2}{18\rho_f\gamma_f};$ $\tau_f = \frac{\gamma_f}{U_\tau{}^2} d_p{}^* = \frac{d_p}{\delta};\ \rho_p{}^* = \frac{\rho_p}{\rho_f}$	Particle shear Stokes number'*' Indicates non-dimensional
σ	Turbulent Schmidt number
τ	SGS Reynolds stress tensor
S	Rate of strain tensor
C_s	Smagorinsky constant
L	Leonard stress tensor
M	Filtered rate-based strain tensor
Δ	Filter width

Subscripts

p	Particle
f	Fluid
T	Terminal
s	Settling
t	Turbulent

and solid particles are modelled using a Lagrangian technique (Baker et al., 2020). While Eulerian-Eulerian methods are useful for flows of any particle volume fraction, their main drawback lies in the assumption that each phase is in local thermodynamic equilibrium, and the difficulty in specifying closures for the prediction of momentum, heat and mass transfer between the phases (Bajpai et al., 2025; González-Lavín et al., 2024). In contrast, Eulerian-Lagrangian techniques become computationally restrictive at the particle volume fractions relevant to many applications.

Studies of particle transport and deposition processes, together with their theoretical modelling using both Lagrangian particle tracking (LPT) and Eulerian approaches to predicting the solid phase, have been conducted for particle-laden flows in pipelines (Yang et al., 2022; Marchioli et al., 2025; Dutta et al., 2022; Messa et al., 2021; Wang et al., 2025). Nevertheless, quantitative assessment of the discrepancies between Lagrangian and Eulerian methods in many flows is still lacking (Zhao et al., 2024). Further research is needed to compare the two approaches across various particle concentrations, and to consider the unique challenges posed by particle-laden flows in different scenarios. More specifically for industrial liquid–solid settling suspensions, the lack of an optimised global approach highlights the need for further research, accounting for diverse factors such as flow dynamics, particle characteristics and pipe geometries.

The Lagrangian approach is frequently used in the simulation of particle suspensions, sprays and bubbly flows, employing techniques such as Reynolds-averaged Navier-Stokes (RANS) equation solution methods, as well as large eddy simulations (LES) and direct numerical simulations (DNS), but is limited to dilute particle concentrations (Han et al., 2019; Savari and Barigou, 2024). Challenges in Lagrangian approaches due to nonuniform particle density are mitigated through refined numerical discretisation, crucial in Eulerian-Lagrangian methods, as well as probability density function (PDF) interpretation in adaptive LPT algorithms (Vegendla et al., 2011). In contrast, the Eulerian-Eulerian technique, is more suitable for large, concentrated multiphase systems, with its shortcoming being the loss of detail necessitating closure equations for turbulence and interaction forces (Heng et al., 2018). Computational demands vary, with the Lagrangian approach requiring significantly more computational resources than the Eulerian approach (Saidi et al., 2014). For the latter methods, mixture models and two-fluid approaches with a drift flux model, or kinetic granular theory, are popular in simulating concentrated solid–liquid flows, although all have different challenges such as numerical instabilities, computational complexity, and difficulties in handling complex geometries.

As an important example, Ekambara et al. (Ekambara et al., 2009) employed the kinematic theory of granular flow and a RANS approach in their CFD simulations of liquid–solid slurry pipe flows, while Kaushal et al. (Kaushal et al., 2012) used a Eulerian-Eulerian two-phase model for predictions of pressure drop and concentration profiles in pipeline slurry flows with high particle concentrations. More recent simulations of liquid–solid slurries predominantly use Eulerian-based models for solids with the kinematic approach coupled to RANS for the turbulent carrier fluid (Chen et al., 2024; Joshi et al., 2025; Tian et al., 2021; Vakilzadeh et al., 2023; Zhang et al., 2022). Though the kinematic approach is less expensive than more advanced techniques, it is generally applied only to dense particle flows as well as being limited due to its assumptions of homogeneity and neglect of particle interactions, and its sensitivity to initial conditions. In these circumstances, modified drift flux models (Zhang et al., 2024) may be crucial in capturing the relative motion between the phases. Moreover, most research studies that conduct Eulerian-Eulerian simulations with high particle concentrations often overlook hindered settling (Yang et al., 2022; Joshi et al., 2025; Chengxi et al., 2024; Rashidi Gugheri and Pakravan, 2025; Wang et al., 2023). However, for accurate predictions, especially at high particle concentrations, accommodation of hindered settling is essential, considering its influence on crucial particle interactions and properties.

RANS is conventionally used in engineering applications due to its relatively short run times, although large eddy simulation (LES) outperforms RANS in terms of accuracy due to its three-dimensional, time-dependent resolution of the large scale energy containing motions within a flow (Hoque et al., 2024; Yang et al., 2014). In this study, LES was chosen for simulating the carrier phase for this reason, as an optimum route to give much greater and more detailed turbulence information than RANS, but without the high computational costs of direct numerical simulation. There is limited use of LES in predicting turbulent pipe flows of segregating slurries (Garg et al., 2024; He et al., 2018), although simulation is the logical choice in nuclear-related applications due to the requirements of high accuracy and reliability. Nevertheless, its application to the flows of interest requires convincing validation against experimental data, where available, as well as results obtained from direct numerical simulations.

The aim of this study is therefore to investigate segregating particle-laden pipe flows using LES in the OpenFOAM® code (Lysenko et al., 2013; Weller et al., 1998). It explores various scenarios, including horizontal and vertical pipe flows with different solid volume fractions (Vreman, 2007; Vreman et al., 2009; Wolde et al., 2023), and the modelling of different types of slurry flow (Yang et al., 2022; Ekambara et al., 2009; Gillies et al., 2004; Kaushal and Tomita, 2007; Yao et al., 2023). To better understand the multiphase flows considered here, a validated LPT is first used to directly compare with an implicit Eulerian-Eulerian approach at low particle volume fractions to confirm the accuracy of the latter model, with the Eulerian-Eulerian approach subsequently allowing extension to intermediate and high-volume fractions. Equilibrium particle concentration profiles are used to establish and compare the dynamic flow behaviour, where discrete sizes of glass particles are used for the simulations. Validation of the predictions is carried out through comparison with results obtained from direct numerical simulations, analytical models and experimental data. High-resolution simulations based on LES for predicting turbulent flows, LPT for tracking discrete particles at low concentrations, and an Eulerian-Eulerian approach for dense suspensions, are used to predict segregating and sedimenting slurry flows. Critically, the influence of hindered particle settling on the sedimentation of particles is studied by the incorporation of a power-law hindered settling model. The novelty in the work arises from the use of LES as the basis for the validated prediction of segregating slurry flows across a large range of particle concentrations, and the impact of hindered settling models on segregation at moderate to high particle concentrations.

2. Methodology

2.1. Fluid phase modelling

Turbulent flow in an incompressible Newtonian fluid is mathematically represented by the Navier-Stokes equations (Elreafay et al., 2025). The current simulations assume pressure-driven, incompressible fluid flow in a circular pipe with constant density. In LES, the fluid flow is separated into large-scale resolved motions and small subgrid-scale fluctuations. Resolving the large, energy containing motions directly, LES is based on a filtering operation to separate the velocity field into two components; the first captures the larger-scale features, while the second necessitates modelling of the unresolved subgrid-scale (SGS) stress tensor to close the equation set.

Equation (1) gives the governing equations for large eddy simulation, derived from the normal filtering operation:

$$\nabla \bullet \overline{\boldsymbol{U}} = 0 \text{ and } \frac{\partial \overline{\boldsymbol{U}}}{\partial t} + \overline{\boldsymbol{U}} \bullet \nabla \overline{\boldsymbol{U}} = -\nabla \overline{\mathbf{P}} + \nu \nabla^2 \overline{\boldsymbol{U}} - \nabla \bullet \tau^{sgs} \quad (1)$$

Where $\boldsymbol{U}$, $\boldsymbol{P}$ and $\boldsymbol{\upsilon}$ denote velocity vector, kinematic pressure (i.e., pressure normalised by constant density), and kinematic viscosity, respectively. Here, overbars indicate the filtered values.

In Eqs. (2), (3) and (4), the subgrid-scale stress tensor τ^{sgs} is related to the rate of strain tensor (S^{-}) of the resolved scale in order to determine the subgrid-scale stress (Vijiapurapu and Cui, 2007; Schmitt, 2007; Sharif Ahmadian and Sharif Ahmadian, 2016):

$$\tau^{sgs} = -2C_s\Delta^2|\overline{\boldsymbol{S}}|\overline{\boldsymbol{S}} \quad (2)$$

$$\overline{\boldsymbol{S}} = \frac{1}{2}\left(\nabla\overline{\boldsymbol{U}} + (\nabla\overline{\boldsymbol{U}})^T\right) \quad (3)$$

$$|\overline{\boldsymbol{S}}| = \sqrt{2\overline{\boldsymbol{S}} : \overline{\boldsymbol{S}}} \quad (4)$$

A method was introduced to dynamically compute the Smagorinsky constant, C_s, based on information from the resolved scales of motion (Germano et al., 1991; Lilly, 1992). Below, an overbar represents grid-filtered values, whilst an overbar with a circumflex represents test-filtered values, with the model constant C_S determined as following Eq. (5). In Eq. (5), Δ denotes the filter width.

$$C_s = -\frac{1}{2}\frac{(\boldsymbol{L}:\boldsymbol{M})}{(\boldsymbol{M}:\boldsymbol{M})}; \text{ where } \boldsymbol{L} = -2C_s\boldsymbol{M} \text{ and } \boldsymbol{M} = \widehat{\Delta}^2|\widehat{\overline{S}}|\widehat{\overline{S}} - \left[\Delta^2\widehat{|\overline{S}|\overline{S}}\right] \quad (5)$$

Test-filtered values result from the application of a second, coarser filter to the already filtered LES equations, which is then used to dynamically compute C_S based on information available at the resolved scale, i.e. the difference between test- and grid-filtered stresses is used to calculate the appropriate amount of dissipation in the flow rather than assuming a constant C_S value.

2.2. Particulate phase modelling

In the simulations, particles are injected randomly, collisions with the pipe wall are elastic, and periodic boundary conditions are applied across the outlet and inlet planes, as for the carrier phase. For two-phase flows, the Navier-Stokes equations are by Eqs. (6) and (7) (Tanguay et al., 2014):

$$\frac{\partial}{\partial t}(\alpha_p\rho_p) + \nabla.(\alpha_p\rho_p\boldsymbol{U_p}) = 0 \quad (6)$$

$$\frac{\partial}{\partial t}\left((1-\alpha_p)\rho_f\boldsymbol{U_f}\right) + \nabla.\left((1-\alpha_p)\rho_f\boldsymbol{U_f}\boldsymbol{U_f}\right) = (1-\alpha_p)\rho_f g - \alpha_f\nabla p + f_{drag}(\boldsymbol{U_f}\boldsymbol{U_f}) + \nabla.\left((1-\alpha_p)\mu_f\left(\nabla\boldsymbol{U_f} + (\nabla\boldsymbol{U_f})^T\right)\right) \quad (7)$$

with the pressure field for each phase assumed identical. Here, α, ρ, μ, g and f_{drag} signify the volume fraction, density, dynamic viscosity, gravitational acceleration and drag force, respectively. Additionally, subscripts p and f represent the particle and fluid, respectively.

The concentration of solid particles (C, g/L) can be calculated using Eq. (8):

$$C = \rho_p\alpha_p \quad (8)$$

To track particle positions over time, to highlight eventual segregation, two different methods were used, Lagrangian particle tracking (LPT) with particle positions resolved explicitly for low concentrations, and a Eulerian drift-flux approximation approach for moderate to high concentration systems, where a specific concentration was chosen as a cross-over point with both methods being correlated directly.

2.2.1. Lagrangian particle tracking

Lagrangian particle tracking provides detailed tracking of individual particle trajectories in the computational domain over time, aiding in understanding complex interactions between the fluid and particles. LPT treats particles as point masses with updated positions and velocities based on differential equations (Zhao et al., 2008; Heinrich and Schwarze, 2020), as shown in Eq. (9):

$$\frac{d\boldsymbol{x}_p}{dt} = \boldsymbol{U}_p \text{ and } \frac{d\boldsymbol{U}_p}{dt} = \boldsymbol{F}_D(\boldsymbol{U}_f - \boldsymbol{U}_p) + \frac{g(\rho_p-\rho_f)}{\rho_p} + \boldsymbol{F}_a = \frac{(\boldsymbol{U}_f - \boldsymbol{U}_p)}{\frac{\rho_p}{\beta}} + \frac{g(\rho_p-\rho_f)}{\rho_p} + \boldsymbol{F}_a \quad (9)$$

The particle response time (τ_p from Stokes Law) can be calculated from Eq. (10):

$$\tau_p = \frac{\rho_p d_p^2}{18\,\mu_f} \quad (10)$$

In Eq. (9), the first term on the right-hand side is the drag force, which is the most significant force in particle-laden flows, playing a pivotal role in determining particle movement and interaction with the fluid. This force acts like a resistive force that opposes the particle's motion, slowing down moving particles through the fluid, and is directly proportional to the relative velocity between the particles and the fluid. The drag force is also essential for calculating the Stokes terminal velocity. The second term of the equation is the gravitational force, which plays a role in determining the trajectory and behaviour of solid particles as they move through fluid in the vertical direction. This is the driving force for sedimentation or flotation that causes particles to either settle or rise in a fluid flow, depending on their density relative to that of the fluid. The last term in Eq. (9) consists of other forces, such as the lift force. In this work, the lift force was neglected as it has a very small effect on the types of flow of interest (Bagchi and Balachandar, 2003).

The term, β, in Eq. (9), is related to the drag coefficient, C_d, the fluid density, ρ_f, the fluid velocity, U_f, and the particle diameter, d_p, i.e. β accommodates the complex interplay between the properties of the particle and the fluid in determining the drag force experienced by the solid particle. Thus, the drag factor is basically an inter-phase momentum transfer coefficient, and can be calculated after Vreman et al. (Vreman et al., 2009), as shown in Eq. (11), where the particle Reynolds number ($\mathrm{Re_p}$) and fluid kinematic viscosity are defined in Eq. (12):

$$\frac{\beta d_p^2}{\mu_f} = \frac{3}{4} C_d \mathrm{Re_p}\,;\; C_d = \left\{ \begin{array}{c} \dfrac{24\left(1 + 0.15\mathrm{Re_p^{0.687}}\right)}{\mathrm{Re_p}};\ \mathrm{Re_p} \le 1000 \\ 0.44;\ \mathrm{Re_p} > 1000 \end{array} \right\} \tag{11}$$

$$\mathrm{Re_p} = \frac{(U_f - U_p)d_p}{\nu_f},\ \nu_f = \frac{\mu_f}{\rho_f} \tag{12}$$

When the particle volume fraction is very low, the influence of particles on the turbulent flow are negligible and the interaction between the fluid and particles can be treated as one-way coupled (the flow influences the particles but not *vice versa*).

2.2.2. Eulerian approach

The Lagrangian approach provides a microscopic view of particle motion by focusing on individual particles and tracking their trajectories, velocities and accelerations. In contrast, the Eulerian approach considers fixed points in space, treating the particles as a continuum, and tracks changes in properties at those points, thereby providing a more macroscopic view. The main advantage of the Eulerian approach for the present application is its suitability for high mass loadings of particles, and the attendant computational run time savings.

When there is significant relative motion between the fluid and particles, this can be accounted for by introducing a source term, S_C, in the concentration conservation equation. This ensures consistency with the general form of transport equations for the fluid, allowing them to be solved together using a unified numerical approach (Zhang and Chen, 2007). In the Eulerian drift flux model, the impact of gravitational settling on particle concentration is considered through the solution of two sets of conservation equations, one for each phase (Zhao et al., 2008; Li et al., 2015; Zhang et al., 2023). In this model (Zhao et al., 2008) the concentration conservation equation is written as:

$$\frac{\partial(\rho_f C)}{\partial t} + \nabla.\left(\rho_f (\boldsymbol{U}_f + \boldsymbol{U}_T) C\right) = \nabla.\left(\frac{\mu_{eff}}{\sigma_f}\nabla C\right) + S_C \tag{13}$$

The drift flux model enhances conventional transport for concentration by incorporating a drift flux term, $\nabla(\rho_f \boldsymbol{U}_T C)$, where the drift flux of solids arises from the velocity difference between particles and fluid due to the drag force and gravity. In Eq. (13), σ denotes the turbulent Schmidt number (typical values 0.7–1). The magnitude of the settling velocity (Li et al., 2015) in non-hindered flows is extracted as the Eq. (14), based on Stokes law:

$$\boldsymbol{U}_T = \left[\left(\frac{4}{3}\right)\frac{g d_p(\rho_p - \rho_f)}{C_d \rho_f}\right]^{0.5} \tag{14}$$

The direction of the settling velocity is directed perpendicularly downwards, in the direction of gravity. Here, C_d depends on $\mathrm{Re_p}$, which is calculated from Eq. (15) and $\mathrm{Re_p} = \frac{U_T \rho_f d_p}{\mu_f}$.

$$C_d = \left\{ \begin{array}{c} \dfrac{24}{\mathrm{Re_p}}\ when\ 10^{-4} \le \mathrm{Re_p} < 1 \\ \dfrac{24}{\mathrm{Re_p}} + \dfrac{3}{\mathrm{Re_p}^{0.5}} + 0.34\ when\ 1 \le \mathrm{Re_p} < 500 - 1000 \\ 0.44\ when\ 500 - 1000 \le \mathrm{Re_p} < 2{*}10^5 \\ 0.10\ when\ \mathrm{Re_p} > 2{*}10^5 \end{array} \right\} \tag{15}$$

2.2.3. Hindered settling models

Hindered settling occurs in slurry pipe flows with moderate to high particle concentrations, where fluid drag interactions between particles hinder their settling velocity. During particle settling in such a flow within a pipe, the displacement of fluid beneath the particles can impede the hindered settling process, potentially modifying the Stokes law terminal settling velocity. The hindered settling velocity (Antonopoulou et al., 2018) is calculated from:

$$\boldsymbol{U_h}(\alpha_p) = \boldsymbol{U}_T f_h(\alpha_p) \tag{16}$$

The hindrance function can be expressed by the Richardson-Zaki relationship (Richardson and Zaki, 1997) and is given by:

$$f_h = (1 - \alpha_p)^{R_z} \tag{17}$$

here, R_z is a constant generally determined experimentally (Johnson et al., 2016; Kramer et al., 2019; Lockwood et al., 2021) and its value is written as in Eq. (18) for different particle $\mathrm{Re_p}$ ranges:

$$R_z = \left\{ \begin{array}{c} 4.65\ when\ \mathrm{Re_p} < 0.2 \\ 4.4\mathrm{Re_p}^{-0.03}\ when\ 0.2 \le \mathrm{Re_p} < 1 \\ 4.4\mathrm{Re_p}^{-0.1}\ when\ 1 \le \mathrm{Re_p} < 500 \\ 2.4\ when\ \mathrm{Re_p} \ge 500 \end{array} \right\} \tag{18}$$

In general, there is no upper concentration bound for the hindered Richardson-Zaki relationship. Thus, a modified hindrance model was also used (Johnson et al., 2016; Hunter et al., 2020) that employs forcing functions, based on the relationship to the maximum volume fraction of particles in a bed ($\alpha_{p,\mathrm{max}}$) to help balance the suspension front, as given in Eq. (19). In all cases, the maximum particle volume fraction was assumed to be 0.64, except for the hindered settling model, based on the loose hexagonal packing limit for spheres. A value of 0.3 maximum volume fraction is used in the hindered case.

$$\left. \begin{array}{c} \mathrm{If}\,\alpha_p < \alpha_{p_{max}}\ \mathrm{then}\,\boldsymbol{U_h}(\alpha_p) = \boldsymbol{U}_T(1-\alpha_p)^{R_z}\left(\dfrac{\alpha_p}{\alpha_{p_{max}}}\right) \\ \mathrm{If}\,\alpha_{p_{max}} \le \alpha_p < 2\alpha_{p_{max}}\ \mathrm{then}\,\boldsymbol{U_h}(\alpha_p) = -\boldsymbol{U}_T(1-\alpha_p{'})^{R_z}\left(\dfrac{\alpha_p{'}}{\alpha_{p_{max}}}\right);\alpha_p{'} = 2\alpha_{p_{max}} - \alpha_p \\ \mathrm{If}\,\alpha_p > 2\alpha_{p_{max}}\ \mathrm{then}\,\boldsymbol{U_h}(\alpha_p) = -4\boldsymbol{U}_T \end{array} \right\} \tag{19}$$

Here, R_z is as defined in Eq. (18).

2.3. Simulation setup

Several fully developed turbulent pipe flows at different Reynolds numbers were considered, all with $L = 12.5D$. Grid elements with hexahedral cells were employed for the simulations and the total number of mesh elements was 1.5 million (see Fig. 1). In the axial direction, the mesh grid elements were evenly spaced, however, in the radial direction near the wall, these elements were specified using a geometric progression, ensuring $\Delta r^{+}_{wall} < 1$ for the first volume next to the wall (Jiang and Lai, 2009). Periodic boundary conditions were imposed in the streamwise direction, while in the normal direction, no-slip boundary conditions were applied to the fluid at the walls.

Particle-laden and unladen pipe flows were initially simulated for a shear Reynolds number, $Re_\tau = 278$, with LES, considering one-way and four-way coupling using OpenFOAM® pimpleFoam and a modified LPT solver (modified pimpleLPTFoam) for comparison purposes. The modified pimpleLPTFoam solver integrated the LPT equations directly into the PIMPLE loop, to enable iterative updates of the momentum exchange terms within each time step, thereby improving numerical stability. Although the modification supports full four-way coupling, most cases were simulated using one-way coupling to maintain computational efficiency, with full four-way interaction selectively applied to a reduced-particle case to capture inter-particle effects. The solver was modified by coupling the LPT position and velocity updates directly within the PIMPLE pressure–velocity correction loop.

Particle concentration profiles were computed with both LPT and Eulerian approaches, using modified pimpleLPTFoam and driftFluxFoam solvers respectively. In the case of LPT, particle volume fractions ≤0.03 vol% were used, and so were in the dilute regime. For each case considered using LPT, particles were introduced at arbitrary positions and followed trajectories influenced by drag and gravity, while lift was neglected. Negating lift force may contribute to unphysical near-wall particle accumulation as discussed by Costa et al. (Costa et al., 2020) and Zahtila et al. (Zahtila et al., 2023) in some systems. However, it is justified in the present study, due to the focus on relatively low Re flows in liquid–solid horizontal pipes, where segregation is expected with negligible lift.

For the Eulerian model, the initial simulated concentration range was varied from 0.03–3 vol%, and thus into the hindered settling regime. Therefore, the hindered settling model was introduced into the modified driftFluxFoam solver, for systems ≥1 vol%. Additional validation runs were completed for very high concentration systems (≤20 vol%). It is also noted, importantly, that for each case fully developed flow was established after 19 s from the initiation time, and after that time particles were injected.

In total, 10 case studies were considered, using various sizes of glass particles with density 2500 kgm^{-3} (41 μm, 50 μm, 60 μm, 77 μm, 90 μm, 125 μm, 165 μm and 480 μm) in different concentration regimes, with the particle density ratio ≥ 2.5 in all cases. Table 1 provides a summary of these test cases, along with their critical particle and fluid properties. For the main hindered settling studies, particle sizes of 41 and 77 μm were selected at two different bulk Reynolds numbers, these being consistent with the experimental study of Rice et al. (Rice et al., 2015) on the pipe flow segregation of glass particles. Other cases were chosen to extend the validation study to different particle concentrations and flow regimes. It is clarified that the initial LES validation was undertaken with gas–solid vertical flows (i.e. without gravity) due to the available DNS data (*Case-I, II & IV*). However, the primary horizontal pipeflow investigations presented in this study focused on liquid-–solid phases (*Case III, Case V–X*) due to the direct comparison with applications in nuclear waste transportation.

3. Results and discussion

3.1. Single phase and multiphase flow validation

Particle-laden and unladen pipe flow validation was undertaken using gaseous flows (*Case I and II* in Table 1), simulated at a shear Reynolds number $Re_\tau = 278$, with results compared to the direct numerical simulations of Vreman (Vreman, 2007). The reference simulation had a bulk Reynolds number of ~5300, based on a centreline velocity, $U_0 = 4\ ms^{-1}$, and pipe diameter $D = 2R_0 = 2$ cm. Vreman's findings were compared to the experimental data of Caraman et al. (Caraman et al., 2003) and Borée and Caraman (Borée and Caraman, 2005) with reasonable agreement found, and so only the DNS predictions are considered here. Fig. 2 shows the present LES results compared to the DNS of Vreman (Vreman, 2007) for the mean streamwise velocity in (A), and the root mean square (rms) of the fluctuating

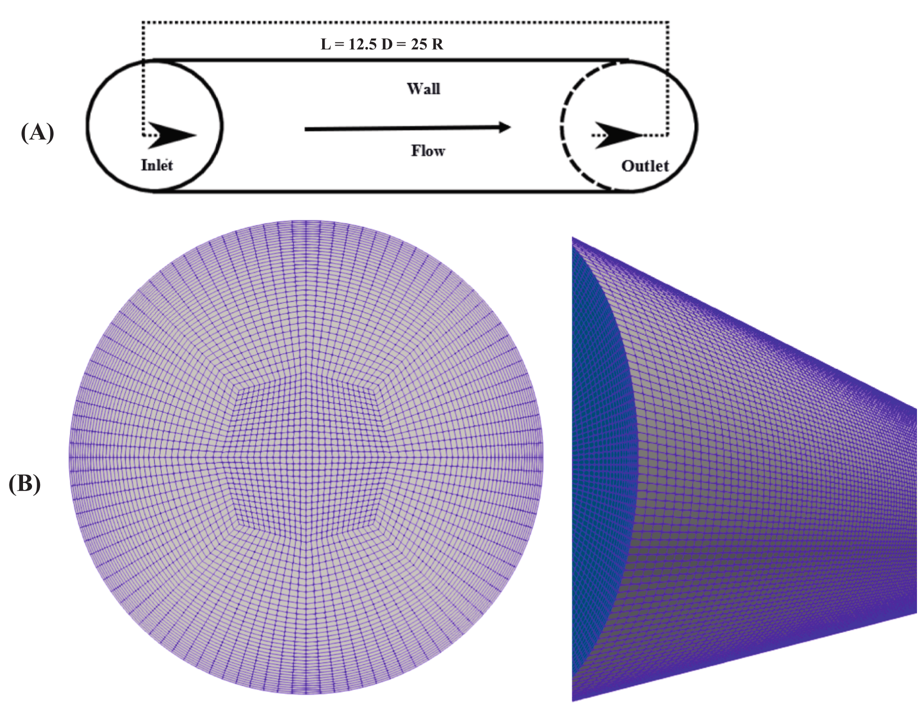

Fig. 1. (A) Schematic of the computational domain and (B) the computational mesh.

Table 1
Summary of simulated test cases.

Case No.	Description	Parameters	References
I	Validation of single-phase pipe flow for shear Reynolds number, $Re_\tau = 278$	Reynolds number ~ 5300 based on centreline velocity $U_0 = 4\ ms^{-1}$	(Vreman, 2007)
II	Validation of multiphase pipe flow for shear Reynolds number, $Re_\tau = 278$ using LPT, comparison of one- and four-way coupling	Particle diameter d_p = 60 μm No. of particles = 29,400 Particle concentration = 0.011 vol% Particle density ratio = 2058 Shear Stokes number, St^+= 79.53	(Vreman, 2007)
III	LPT simulations for shear Reynolds number, $Re_\tau = 2378$	Particle diameter d_p = 77 μm No. of particles = 1,000,000 One-way coupling Particle concentration = 0.03 vol% Particle density ratio = 2.5 Shear Stokes number, $St^+ = 2.57$	
IV	Validation of simulation with DNS data using LPT and Stokes number effect on particle settling for shear Reynolds number, Re_τ = 720	Particle diameter d_p = 50 μm No. of particles = 105,000 Particle concentration = 0.07 vol% Particle density ratio = 7.71 and 23.3 Shear Stokes numbers, $St^+ = 5.55$ and 16.78	(Wolde et al., 2023)
V	Comparison of present Eulerian and LPT findings for shear Reynolds number, Re_τ = 2378	Particle diameter d_p = 77 μm Particle concentration = 0.3 vol% Particle density ratio = 2.5 Shear Stokes number, $St^+ = 2.57$	
VI	Eulerian particle settling model for shear Reynolds number, Re_τ = 2378	Particle diameter d_p = 41 μm and 77 μm Particle concentration = 0.5, 1 and 3 vol% Particle density ratio = 2.5 Shear Stokes numbers, $St^+ = 0.73$ and 2.57	
VII	Comparison of present Eulerian model predictions with different experimental data with different shear Reynolds, $Re_\tau = 2378$, 11461, 6609, 7650 and 7044	Particle diameter d_p = 77 μm, 90 μm, 125 μm, 165 μm and 480 μm Particle concentration = 1, 3, 8.4, 9.18, 19 and 20.3 vol% with different flow velocities (1.25 ms^{-1}, 3 ms^{-1} and 3.44 ms^{-1}) Particle density ratio = 2.5 Shear Stokes numbers, $St^+ = 2.57$, 13.93, 31.45, 83.43 and 598.65	(Gillies et al., 2004; Rice et al., 2015; Roco and Shook, 1983)
VIII	Comparison of Eulerian particle settling model with hindered settling approach to non-hindered approach for shear Reynolds number, $Re_\tau = 2378$	Particle diameter d_p = 77 μm Particle concentration = 1, 3, 5, 7 vol% Particle density ratio = 2.5 Shear Stokes number, $St^+ = 2.57$	
IX	Comparison of Eulerian particle settling model using two hindered settling approaches for shear Reynolds number, $Re_\tau = 2378$	Particle diameter d_p = 77 μm Particle concentration = 7 vol% Particle density ratio = 2.5 Shear Stokes number, $St^+ = 2.57$	
X	Comparison of Eulerian particle settling model with hindered settling approach to different experimental data	Particle diameter d_p = 90 μm and 125 μm Particle concentration = 19 and 20 vol% with different diameters of pipes	(Gillies et al., 2004; Kaushal and Tomita, 2007)

velocities ($U_z{}^*{}_{,\,rms}$ in the axial, *z*, and $U_r{}^*{}_{,\,rms}$ in the radial, *r*, directions), and the Reynolds shear stress $<U_zU_r>$ in (B), where $U^* = U/U_0$. Fig. 2 (B) also shows the normal stress in the circumferential, *θ*, direction, although values of this stress were not provided in Vreman (Vreman, 2007).

The present LES demonstrates good agreement with the DNS results, for both the mean velocity and turbulence statistics, especially near the wall where high levels of turbulence are found. There are some slight discrepancies beyond the wall region that occur in the bulk of the flow where the flow characteristics are dominated by large and very energetic scales of fluid motion, resolved by both the LES and DNS. These differences are likely due to the grid resolution used in the present work compared to Vreman (Vreman, 2007). Despite these minor differences, the close agreement validates the LES approach employed in this study.

For particle-laden pipe flow validation, a modified Lagrangian particle tracking solver (modified pimpleLPTFoam) was employed with the LES, using glass beads as solid particles (*Case II* in Table 1), as considered by Vreman (Vreman, 2007). The gravitational force was aligned with the mean fluid (air) flow (i.e. vertically) and was applied in both one- and four-way coupled computations, maintaining identical solid-particle characteristics for both cases. Predictions are compared with the DNS-LPT results of Vreman (Vreman, 2007) in Fig. 3.

Good agreement is found between the present LES-LPT predictions and those of Vreman (Vreman, 2007) for both the continuous and particle phases when four-way coupling is employed. It is observed that the continuous phase is only slightly affected by the particle phase in moving from one- to four-way coupling, although clearly this has a significantly large impact on the normal stresses. Importantly, the four way coupled results present a higher peak in U_z rms within the near-wall region for the particle phase (in line with the DNS) suggesting turbulence enhancement, likely caused by the high-inertia particles generating wakes and vortex shedding, injecting kinetic energy into the fluid. For both the fluid and the particles, the mean streamwise velocities are well predicted close to the wall and in the bulk flow region, although there is again a slight over-prediction of the mean velocities just beyond the wall region, likely caused by the noted grid resolution differences. Close agreement is also found with the DNS results for the particle normal and shear stresses when four-way coupling is used. The use of LES to predict pipe flows may therefore be considered to provide a realistic representation of the turbulent velocity field, with LES-LPT results also in line with available DNS-based predictions for the solid phase. Thus, the overall approach a reliable choice for the subsequent prediction of lower Reynolds number particle-laden flows in horizontal pipes that lead to segregating, partially sedimented behaviour.

3.2. Particle concentration profiles

Fig. 4 shows the prediction of the LES with LPT (*Case III* in Table 1), where the modified LPT solver was used to perform the liquid–solid pipe

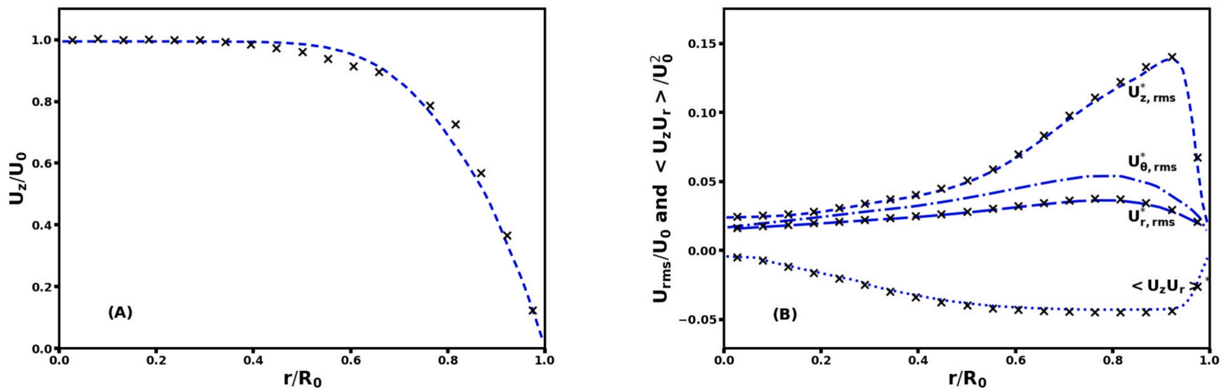

Fig. 2. Single-phase flow validation: (A) mean streamwise velocity; and (B) rms of fluctuating velocities and Reynolds shear stress. Dashed/dotted lines – LES, × Vreman (Vreman, 2007) DNS.

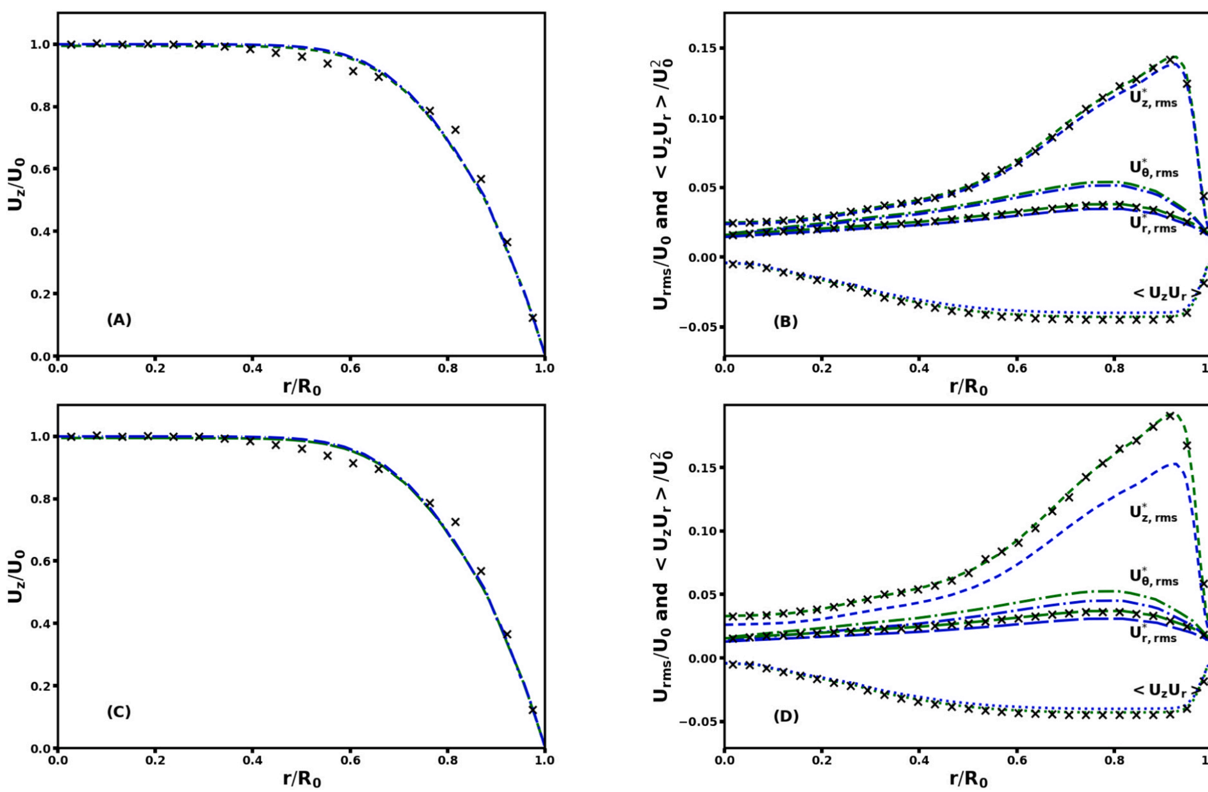

Fig. 3. Multiphase flow validation: (A) mean streamwise velocity; (B) rms of fluctuating velocities and Reynolds shear stress; (C) particle mean streamwise velocity; and (D) particle rms fluctuating velocities and Reynolds shear stress. Dashed/dotted blue lines – current LES (one-way coupled), dashed/dotted green lines – LES (four-way coupled), × Vreman (Vreman, 2007) DNS (four-way coupled).

flow simulation. The velocity profile and contour plot, as well as the velocity rms and Reynolds shear stress statistics of the fully developed flow (prior to particle injection) are given within the Electronic Supplementary Materials (ESM), Figs. S-1 and S-2.

Fig. 4 (A) presents instantaneous plots of particle position along a vertical plane in the streamwise and spanwise directions at four simulation times, while Fig. 4 (B) shows particle concentration profiles at the same times, normalised by the initial concentration (C/C_0). It is noted again that the particles were injected after 19 s, when the flow had stabilised and reached steady state. From Fig. 4 (A), it can be always observed that the distribution of solid particles is asymmetrical along the vertical plane passing through the centre of the pipe and was broadly symmetrical in the equivalent horizontal plane (although not shown). The higher concentrations are in the lower half of the pipe, where the solid particles tend to settle with time due to gravitational effects. This leads to a segregation of the particles and the formation and growth of a particle bed at the bottom of the pipe (Zhang et al., 2021; Yao et al., 2023; Rice et al., 2015; Ofei and Ismail, 2016). For the flow Reynolds number and particles considered, particle segregation is to be expected (Rice et al., 2015). The results of Fig. 4 (B) demonstrate that the particle settling eventually leads to an equilibrium balance after approximately 60 s. At $y/D \geq -0.3$, particle concentrations are also approximately uniform, but below the initial concentration, and at $y/D \leq -0.3$, particles preferentially accumulate in an increasing concentration band (Wang et al., 2019). In addition, it is noted that the density ratio here was ~ 2.5, and representative of flows typical of natural sands and many industrial minerals engineering processes. For comparison, Cui et al. (Cui et al., 2025; Cui et al., 2026) investigated deposition in particle-

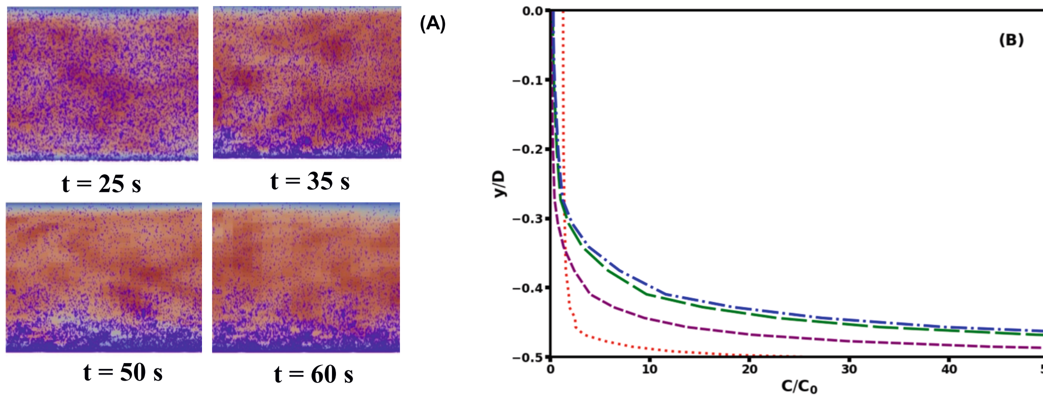

Fig. 4. LES-LPT predictions of 77 μm diameter glass particles at initial concentration of 0.03 vol% in a $Re_\tau = 2378$ flow: (A) Instantaneous plots of particle position within the full pipe; and (B) normalised mean particle concentration in the lower half of the pipe at $t = 25$ s (red), 35 s (purple), 50 s (green) and 60 s (blue).

laden flows with very small density ratios (∼1.05) and still observed concentration segregation at similar Reynolds numbers. Therefore, with the higher density ratios used in the present study, more pronounced sedimentation would be expected.

Given the lack of experimental data at similar concentrations to those considered in this case, validation of the LES-LPT approach was performed against the DNS-LPT predictions of Wolde et al. (Wolde et al., 2023) who considered a turbulent gaseous pipe flow at $Re_\tau = 720$. Particle deposition was also observed by the latter authors, where an initial uniform particle concentration at a volume fraction of 0.07 vol%, and with particle Stokes numbers of 5.55 and 16.78, were considered. Fig. 5 compares particle concentration profiles with time for both sets of simulations (*Case IV* in Table 1). These results demonstrate good agreement between the two approaches, and a similar deposition rate of particles towards the bottom of the pipe with time. Clearly, higher near-wall concentrations occur for the $St^+ = 16.78$ particles when compared to the lower Stokes number case, $St^+ = 5.55$, as the latter particles segregate more slowly as their movement is more governed by viscous forces so that they follow the fluid streamlines more closely and thus segregate less. In comparison, the particles with the higher Stokes number are more inertial such that they depart from the fluid streamlines and settle more rapidly.

As previously noted, Eulerian-Lagrangian techniques become computationally restrictive at the particle volume fractions relevant in many applications and, due to such constraints, the present LES-LPT predictions were limited to a maximum particle concentration of 0.3 vol%. To simulate higher concentration flows, the Eulerian-Eulerian method coupled to a modified drift flux model (driftFluxFoam) was used in OpenFOAM®. Fig. 6 presents a direct comparison of the distance-averaged concentration profiles with height for the LPT and Eulerian-based simulations for the sedimentation of glass particles (*Case V* in Table 1) at the crossover particle concentration of 0.3 vol%. The Eulerian solver predicts a near-wall concentration ratio that is close to that of the LPT, although further away from the wall ($y/D > -0.3$) it underpredicts the extent of particle segregation, essentially indicating the drift flux model predicts slightly less near-wall deposition. This may

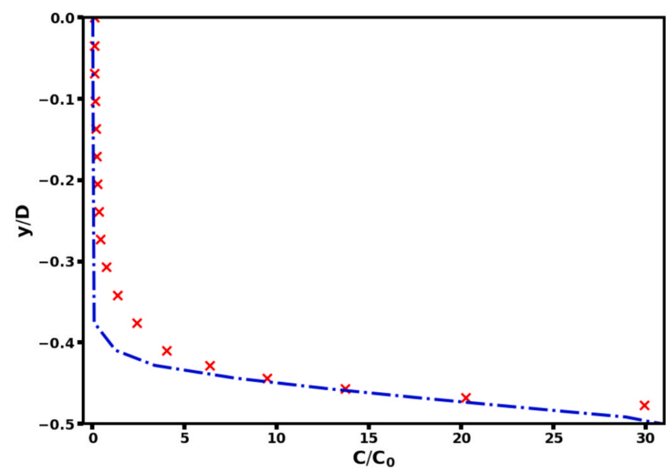

Fig. 6. Comparison of LPT and Eulerian predictions of normalised mean particle concentration in lower half pipe for 77 μm diameter glass particles at initial concentration of 0.3 vol% in a $Re_\tau = 2378$ flow. Dashed/dotted blue line – Eulerian, × – LPT.

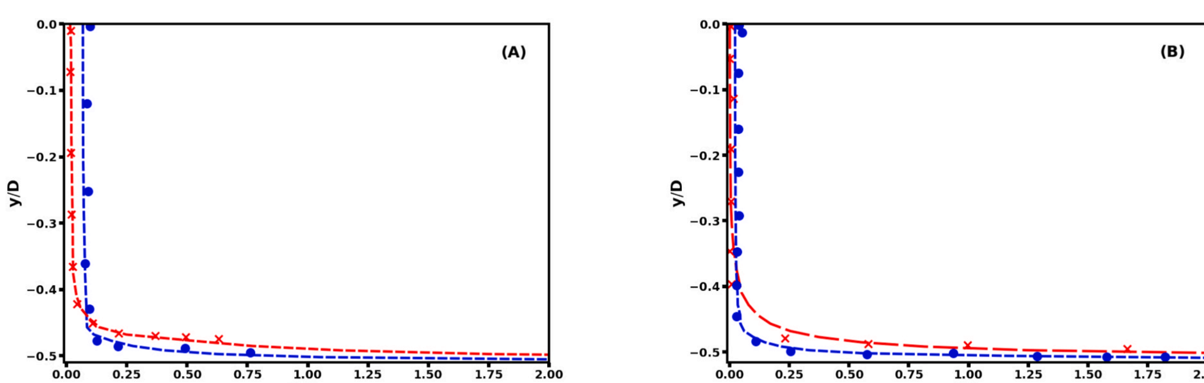

Fig. 5. Comparison of DNS-LPT and LES-LPT predictions of normalised mean particle concentration in the lower half of the pipe for $St^+ = 5.55$ (blue) and $St^+ = 16.78$ (red) particles at: (A) t = 39 s; and (B) t = 69 s. Dashed lines – LES-LPT, × / • Wolde et al. (Wolde et al., 2023).

be due to the defined maximum packing fraction in the Eulerian model although, overall, the correlation between the two solution methods is close, particularly at distances close to the wall. The Eulerian method is therefore used to predict higher particle volume fraction flows of greater industrial relevance.

The Eulerian particle solver, without hindered settling, was subsequently used to predict the sedimentation of two sizes of glass particles (41 and 77 μm diameter) at low-to-intermediate concentrations of 0.5, 1.0 and 3.0 vol% (*Case VI* in Table 1). Fig. 7 shows example concentration contour plots across the pipe at four simulation times ($t = 25$, 35, 50, 60 s) for the three concentrations, with Fig. 8 giving the distance-averaged concentration profiles with height at the same times.

Over time, the particle concentration contours in Fig. 7 confirm the migration of particles to the lower regions of the pipe, with the particles ultimately accumulating at its base as a solid bed. For both cases, the concentration contours stabilise at ~ 60 s, consistent with the previous LPT predictions at lower volume fractions. However, due to the higher volume fractions considered here, the particle concentrations in the near-wall region of the pipe suggest complete deposition of particles and the formation of a dense particle bed. Also, there are significant differences between predictions for the two particle sizes, with consistently higher levels of segregation and bed build-up evidenced with the larger 77 μm diameter particles, as would be expected given their size. It is also noteworthy that the general patterns of segregation are similar for each particle volume fraction, although the consolidated bed size increases with fraction. These patterns align with expectations for liquid–solid multiphase pipe flows and are consistent with previous findings (Ekambara et al., 2009; Kaushal et al., 2012; Ofei and Ismail, 2016).

The particle concentration profiles in Fig. 8 exhibit similar behaviour. That is, with increasing time, the solid concentration increases in the lower regions of the pipe while particles are depleted relative to the mean at intermediate heights. It is evident, as would be expected, that the larger particles produce more segregated concentration profiles (greater C/C_0 ratios in the near-bed region). It is also observed that for higher concentrations, the relative level of segregation is reduced. For example, in the case of the 41 μm diameter particles, Fig. 8C(i) shows that at the highest concentration (3 vol%), the normalised maximum relative solid concentration is 7, whereas a value of 25 occurs for the lowest concentration (0.5 vol%) in Fig. 8A(i). Similarly, Fig. 8C(ii) for the 77 μm particles give a maximum relative concentration of 20 compared to a value of >50 at lower concentrations (Fig. 8A(ii)). Therefore, while the flux of depositing particles is greater at higher concentrations, the relative separation of sedimented particles relative to those in the bulk flow is reduced. This reduction in relative segregation with increases in particle volume fraction is consistent with previous work (Ekambara et al., 2009; Kaushal et al., 2012; Yao et al., 2023; Rice et al., 2015; Ahmed and Mohanty, 2018; Arolla and Desjardins, 2015; Capecelatro and Desjardins, 2013; Rice et al., 2015). It is noted that Yang et al. (Yang et al., 2022) also showed that at higher concentrations (31 vol%), the normalised maximum relative solid concentration reduced to 1.2, whereas the value was greater than 2 at lower concentrations (6 vol%).

Fig. 9 shows profiles and contour plots of the fluid mean velocity for the LES simulations coupled with the Eulerian approach (*Case VI* in Table 1). These results demonstrate that the fluid velocity is affected by the solid particles since the Eulerian approach is inherently two-way coupled. The maximum velocity is therefore found in the upper part of the pipe and not at its centre, while the velocity profile becomes increasingly asymmetrical with increasing segregation (not shown). Two further cases for larger concentrations and velocities are given in the ESM (Fig. S-3), highlighting the asymmetry in the mean velocity profiles. These compare well with previous experimental studies (Gillies et al., 2004; Roco and Shook, 1983) and simulations (Ekambara et al., 2009). This asymmetry in the velocity for liquid–solid flows predicted using Eulerian-Eulerian approaches is also consistent with previous work (Ekambara et al., 2009; Yao et al., 2023; Ofei and Ismail, 2016; Ahmed and Mohanty, 2018).

Other turbulent pipe flows were also investigated by analysing concentration profiles obtained in reference works (Gillies et al., 2004; Rice et al., 2015; Roco and Shook, 1983) (*Case VII* in Table 1). As a representative example, Fig. 10 presents the results from Eulerian-Eulerian simulations compared with the experimental data of Rice et al. (Rice et al., 2015) at two different particle volume fractions for two sizes.

The LES simulations using the Eulerian approach show reasonably good agreement with the experimental data in Fig. 10. The comparison is very good for the larger particles, while the level of segregation predicted by the simulations appears to be greater than the experiments for the smaller particles, resulting in larger particle concentrations at the bottom of the pipe, and more depletion from the middle regions of the

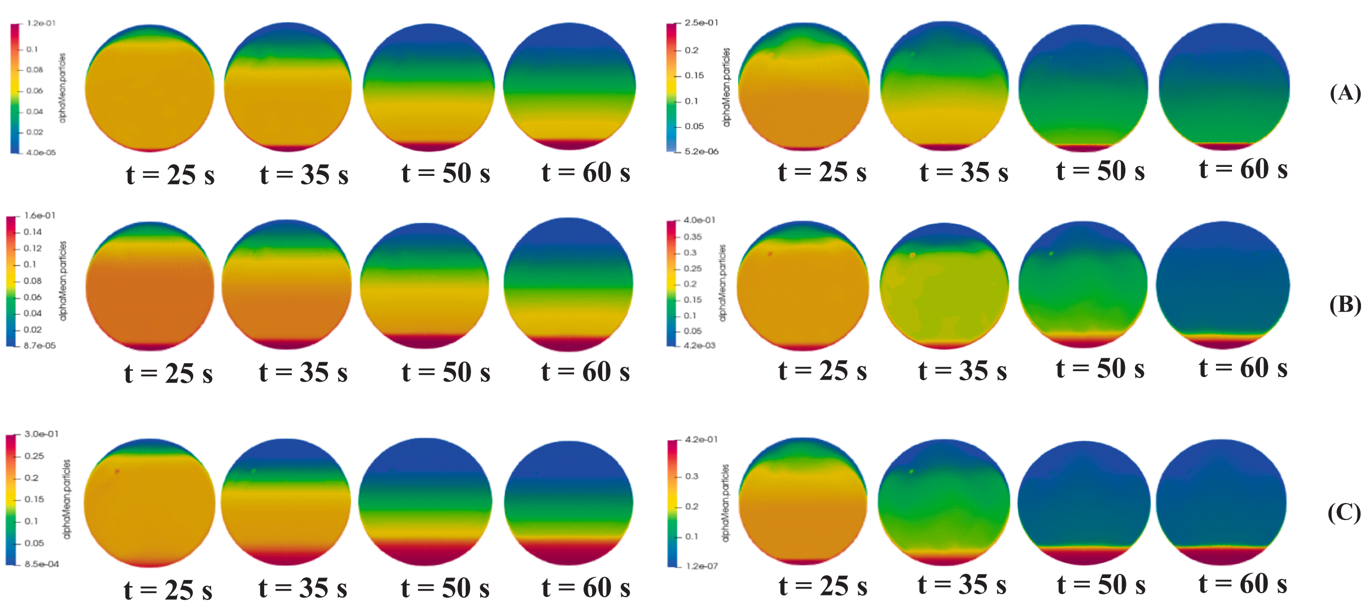

Fig. 7. Contour plots at different times of normalised mean particle concentration across the whole pipe for $Re_\tau = 2378$: (A) $C_0 = 0.5$ vol%, (B) $C_0 = 1.0$ vol%, and (C) $C_0 = 3.0$ vol%; 41 μm diameter particles (left) and 77 μm diameter particles (right).

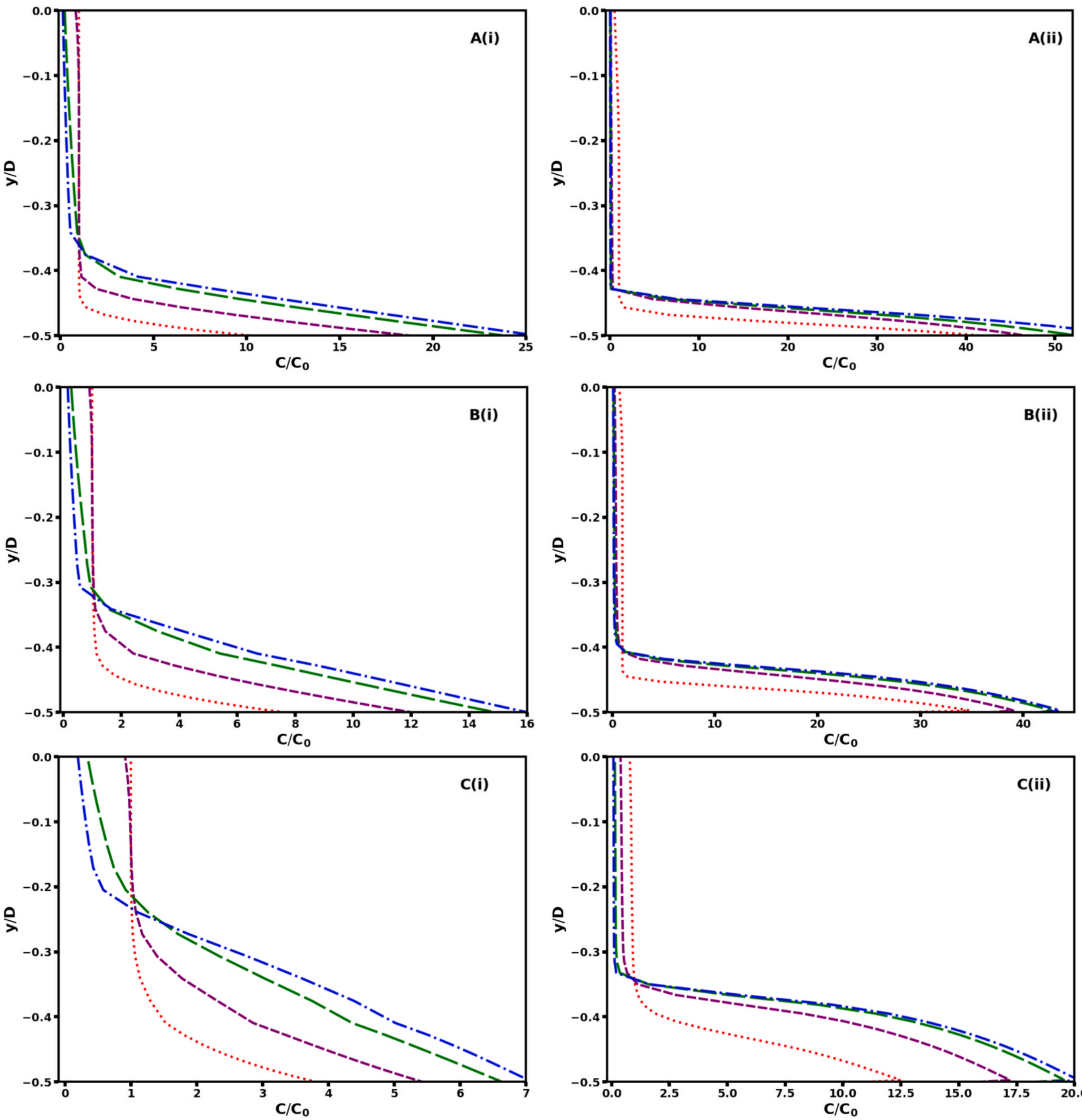

Fig. 8. Eulerian predictions of normalised mean particle concentrations in the lower half of the pipe for $Re_\tau = 2378$ flow: (A) $C_0 = 0.5$ vol%, (B) $C_0 = 1.0$ vol%, and (C) $C_0 = 3.0$ vol%; (i) 41 μm diameter particles and (ii) 77 μm diameter particles; t = 25 s (red), 35 s (purple), 50 s (green), and 60 s (blue).

pipe. Nevertheless, these discrepancies could be partly due to the fact that the experimental data were gathered in a flow loop that was recycled via a mixer (Rice et al., 2015). Thus, experimentally, particles did not get re-introduced at the inlet in the same position as the outlet (as conducted in the simulations) because the slurry was re-mixed into a charge tank before being pumped again through the loop. Thus, the effective experimental time to establish a consistent profile was only 5 s (being the length of time for the slurry to be transported around the flow loop to the measurement point, before ejection back to the charge tank). Hence, the concentrations measured experimentally may not represent true equilibrium profiles – noting the simulations showed that equilibrium was approached after ~ 30 s from particle insertion. The closeness of the profiles for the larger particles, suggests the smaller particles take longer to obtain stable profiles (which would be expected, given their smaller gravitational influence).

To further probe the robustness of the LES-Eulerian simulations, higher particle volume fraction simulations were compared to experimental findings for large 165 μm diameter particles at conditions judged to be closer to equilibrium (Roco and Shook, 1983), as shown in ESM Fig. S-4. Generally, the measurements and predictions compare well, although in the near-wall region there are some minor disparities that could be due to insufficient consideration of forces within the simulations, such as particle–wall interactions, turbulent dispersion and inter-particle collisions that affect the particle concentration profiles (Boutsikakis et al., 2020; Duque-Daza et al., 2021). In Fig. S-2(B), a slight over-prediction of the experimental concentration profile is also observed in the lower part of the pipe ($y/D \leq -0.4$) that again may be a consequence of near-wall modelling challenges and the neglect of the lift force in the simulations (Capecelatro and Desjardins, 2013; Capecelatro and Desjardins, 2013).

It should also be noted that the above simulations did not explicitly consider the hindered settling of the particles, which may become significant at higher particle volume fractions. Hindered settling occurs due to the upward flow of relocated fluid initiating surplus drag on the

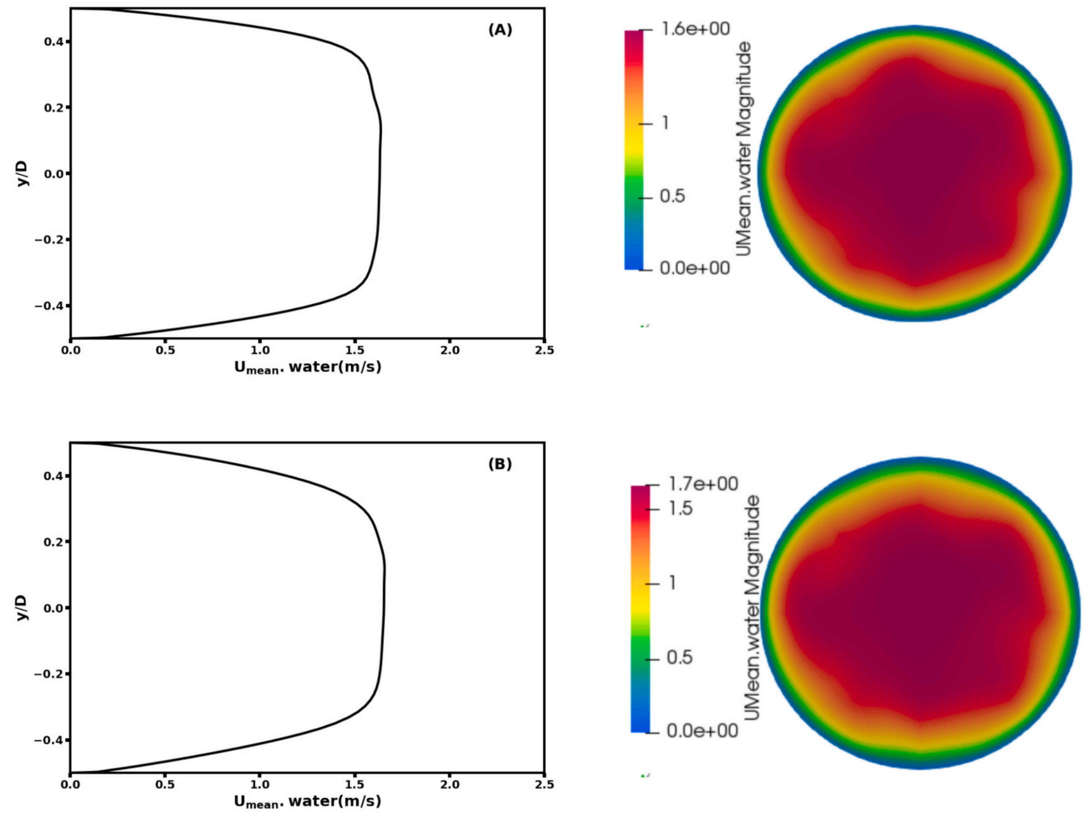

Fig. 9. Profiles and contour plots of fluid mean velocity for Eulerian simulations: $U_0 = 1.25$ ms^{-1}, $C_0 = 3$ vol%, $D = 42.6$ mm and $Re_\tau = 2378$; (A) 41 µm diameter particles and (B) 77 µm diameter particles.

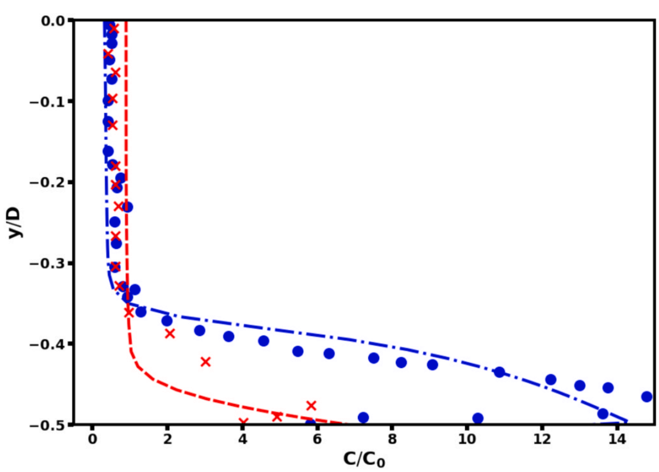

Fig. 10. Eulerian predictions of normalised mean particle concentrations in the lower half of the pipe for 77 µm diameter particles in a $Re_\tau = 2378$ flow: $C_0 = 1$ vol%, 41 µm diameter particles (red) and 3 vol%, 77 µm diameter particles (blue); Dashed/dotted lines – Eulerian, × / • Rice et al. (Rice et al., 2015).

settling solid particles, and numerous inter-particle collisions that increase frictional resistance. Consequently, as particle volume fraction increases, the effective settling velocity decreases due to these interactions, making their incorporation in simulations important to the accurate prediction of the behaviour of particle-laden pipe flows such as in slurry pipelines and sedimentation tanks. For example, previous CFD results of Ekambara et al. (Ekambara et al., 2009) and Capecelatro et al. (Capecelatro and Desjardins, 2013; Capecelatro and Desjardins, 2013) found deviations from experimental findings with higher particle concentrations. Additionally, the fact that the experimental data of Rice et al. (Rice et al., 2015) appears less segregated than the current predictions may also be due to the influence of hindered settling. Thus, it is important to consider the inclusion of a hindered settling model to improve predictive accuracy, as considered in the following section.

3.3. Comparison of slurry segregation with and without hindered settling

LES was performed of higher volume fraction particle flows using the Eulerian approach, inclusive of a hindered settling model using the modified driftFluxFoam solver (*Case VIII* in Table 1). Fig. 11 compares example concentration contour plots across the pipe at 60 s of simulation time for the four concentrations considered (1, 3, 5 and 7 vol%). These runs were carried out with and without the hindered settling model for the case of 77 µm diameter glass particles. Additionally, Fig. 12 compares normalised mean concentration profiles for the same simulations at four example simulation times ($t = 25$, 35, 50 and 60 s).

From Fig. 11, the 60 s contour plots illustrate that qualitative differences in the bulk flow between the hindered and non-hindered settling predictions are relatively minor. However, in the near-bed region, segregation is less pronounced in the hindered settling case, which is more evident visually for the higher volume fractions. When considering changes with time (Fig. 12), particles again approximately reach equilibrium within 50–60 s (noting the similarity of these profiles), which is true for both the hindered and non-hindered settling simulations, and consistent with previous results. Also, the relative level of segregation reduces as the particle volume fraction increases. Nevertheless, the hindered settling model considerably reduces particle segregation, with consistently lower C/C_0 ratios in the lower pipe region. For the lower particle volume fractions (1 and 3 vol%), the hindered and non-hindered settling predictions are similar in most regions of the pipe, although, the build-up of particles is much closer to the base of the pipe with hindered settling, with significant differences occurring for $y/D < -0.4$. For the higher concentrations, differences become

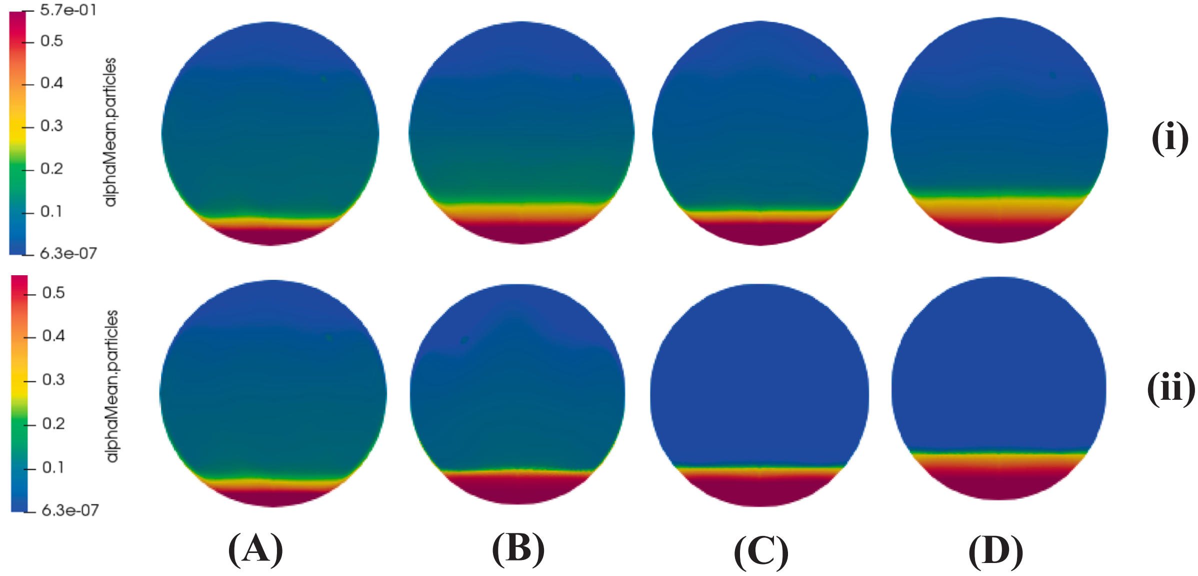

Fig. 11. Contour plots of normalised mean particle concentration for 77 μm diameter particles at $\mathrm{Re}_\tau = 2378$: (A) $C_0 = 1$ vol%; (B) $C_0 = 3$ vol%; (C) $C_0 = 5$ vol%; and (D) $C_0 = 7$ vol%, at $t = 60$ s. Shown (i) with and (ii) without hindered settling.

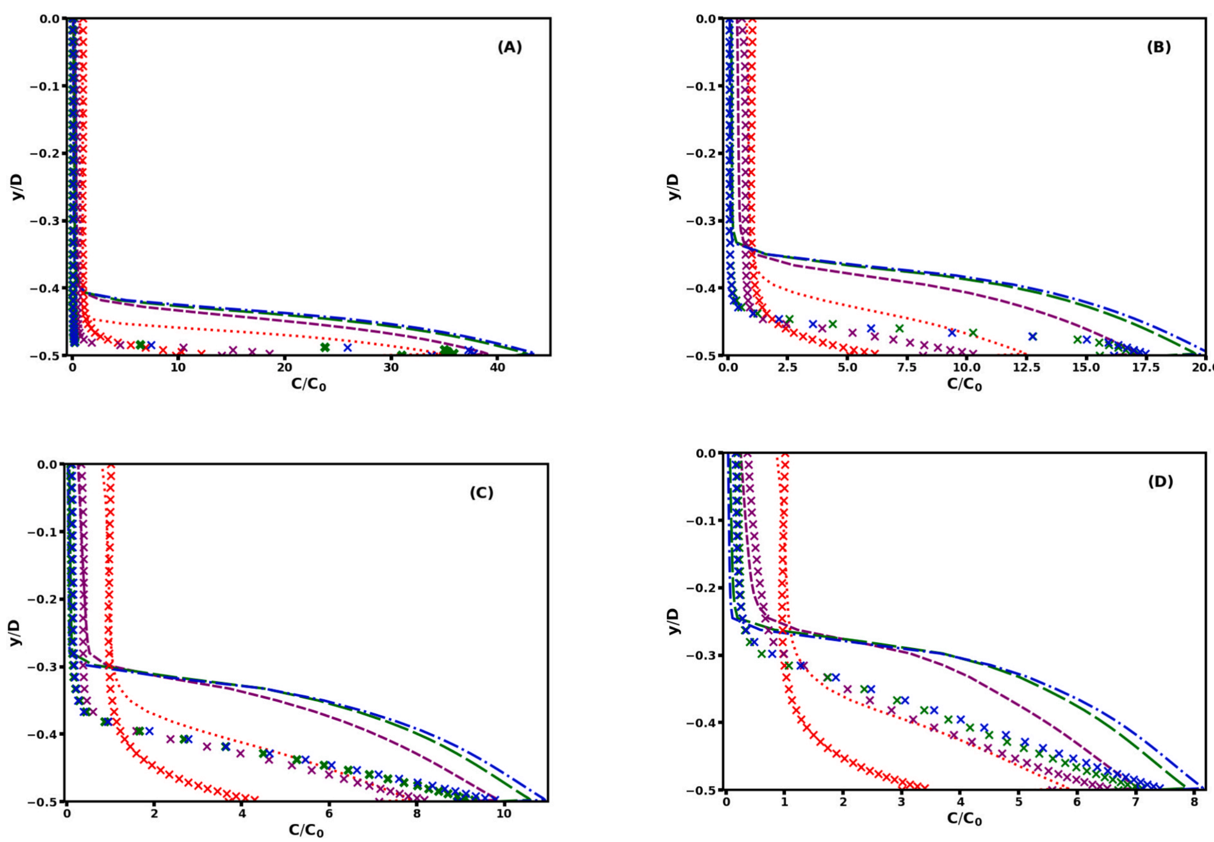

Fig. 12. Normalised mean particle concentration in the lower half of the pipe for 77 μm diameter particles in a $\mathrm{Re}_\tau = 2378$ flow: (A) $C_0 = 1$ vol%; (B) $C_0 = 3$ vol%; (C) $C_0 = 5$ vol%; and (D) $C_0 = 7$ vol%, at $t = 25$ s (red), 35 s (purple), 50 s (green) and 60 s (blue); dashed/dotted lines – without hindered settling, × with hindered settling.

evident at greater heights ($y/D < -0.3$). Also, with the increase in particle volume fraction, interactions with the supernatant liquid and other solid particles become dominant. These modify the segregation behaviour producing a more gradual increase in particle concentration as the pipe base is approached below $y/D = -0.3$, rather than the steep increase in concentration for the non-hindered cases.

To better understand the reliability of the hindered settling model, a comparison was made between the base case Richardson-Zaki power-law function, and the modified model with velocity forcing functions (Hunter et al., 2020), given in Eq. (19), for the same particles at a concentration of 7 vol% (*Case IX* in Table 1). Fig. 13 compares concentration profiles for these two hindered settling model simulations at

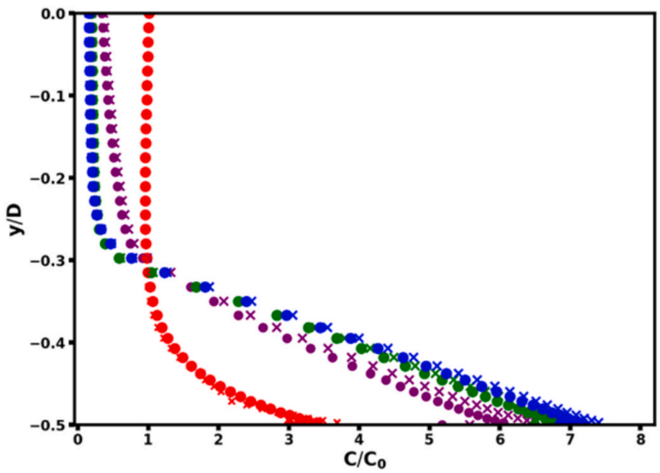

Fig. 13. Normalised mean particle concentration in the lower half of the pipe for 77 μm diameter particles at $Re_\tau = 2378$: $C_0 = 7$ vol% at t = 25 s (red); 35 s (purple); 50 s (green); and 60 s (blue). × Eulerian model with Ricardson-Zaki hindered settling, Eq. (17); • modified hindered settling model, Eq. (19).

four example simulation times ($t = 25$, 35, 50 and 60 s). The two models behave almost identically, although there is a very slight reduction in particle segregation in the near-wall region for the modified model, which stabilises the particles close to the maximum packing fraction. These results therefore demonstrate that the power-law Richardson-Zaki model used in the simulations is robust, even though it does not include a specific upper bound for high concentrations approaching (or above) the packing limit. This is at least true in the current simulations where segregation is relatively low, due to the high levels of turbulence, such that the particles do not approach the packing limit. For other cases at lower velocities (e.g., in settling tanks) modifications to account for limits around the particle maximum packing fraction will become more important (Hunter et al., 2020).

To further validate the Eulerian model with hindered settling, additional simulations for high concentrations were performed (*Case X* in Table 1) and comparisons made with the experimental data of Gillies et al. (Gillies et al., 2004) and Kaushal and Tomita (Kaushal and Tomita, 2007), as shown in Fig. 14. These cases represent very high concentration conditions (C_o – 20 vol%) where hindered settling effects would be maximised. In the flows considered in Fig. 14, it is evident that concentration segregation is minimised due to hindered settling, but it is still noticeably present (with greater C/C_o variation for the larger 125 μm) with very close agreement between the LES and experimental data.

The current LES-Eulerian drift flux simulations coupled to the hindered settling model compare favourably with previous studies, where hindered settling was neglected, or the turbulent flow was modelled with RANS techniques. For example, Ekambara et al. (Ekambara et al., 2009) undertook hydrodynamic simulations of slurry pipeline flow using a k-ϵ based RANS model, performed using an Eulerian kinematic theory of granular flow approach for the particles. However, the kinematic approach simplifies particle interactions, disregarding important collisional and frictional effects that can affect model performance, as well as being limited to certain particle sizes and dilute concentrations that assume binary collisions (Khalilitehrani et al., 2014). Kaushal et al. (Kaushal et al., 2012) also conducted slurry pipe flow simulations using a RANS-based Eulerian-Eulerian approach for high particle volume fractions, although they did not include a hindered settling model, in common with most other previous studies using CFD for high particle volume fraction flows (Dixit et al., 2023; Sadeghi et al., 2022; Shajahan et al., 2024; Yang et al., 2022; Zhang et al., 2021; Zheng et al., 2020).

Conversely, the modified drift flux model is superior for dense flows with high particle volume fractions and multiple interactions between solid particles and, by using a power-law hindered settling model, offers a relatively computationally efficient approach (Abam et al., 2021; Pal, 2019; Turney et al., 2018) that is versatile across differing boundary conditions and a nuanced representation of liquid–solid interactions. Despite requiring additional closure models for particle–particle interactions, its accuracy when compared to experimental data make it an obvious choice for understanding solid particle behaviour in complex flow regimes. It provides a more comprehensive treatment of diffusive transport as well as capturing the relative motion between phases and is suitable for the prediction of both dilute and dense particle flows.

4. Conclusions

This research investigated segregating particle-laden pipe flows using LES in OpenFOAM®. For simulating these flows, numerical strategies employing both Eulerian-Lagrangian and Eulerian-Eulerian frameworks were developed and investigated. To assess the behaviour of particle dispersion, a modified LPT solver was employed to directly track the dispersed solids, with the particles initially inserted at arbitrary locations within a fully developed turbulent liquid flow and assigned the local fluid velocity at those locations. A cyclic boundary condition was applied in the streamwise direction with no-slip conditions at the pipe walls. Statistical data were gathered for analysis after the particle phase had adjusted to the flow. A modified Eulerian solver with a hindered settling model was also developed to predict these flows, with particle concentration profiles compared with those predicted using the particle tracking method and a range of experimental

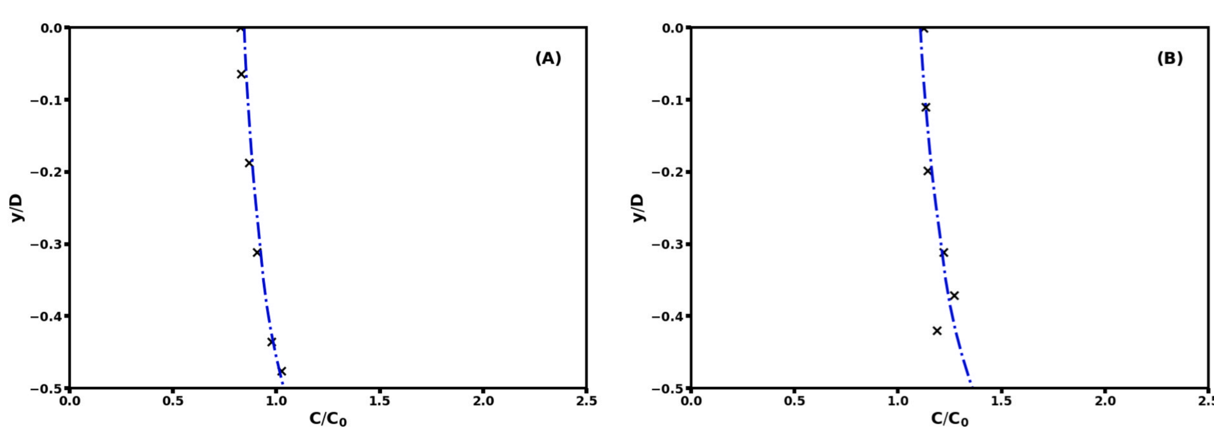

Fig. 14. Normalised mean particle concentration in lower half of the pipe: (A) $C_0 = 19$ vol%, 90 μm diameter particles, $U_0 = 3$ m/s, D = 103 mm, $Re_\tau = 11461$; and (B) $C_0 = 20$ vol%, 125 μm diameter particles, $U_0 = 3$ m/s, D = 54.9 mm, $Re_\tau = 7044$. Dash/dotted lines – Eulerian with hindered settling, × Experimental data (Gillies et al., 2004; Kaushal and Tomita, 2007).

data at industrially relevant volume fractions. A modified driftFluxFoam solver was used as the basis of the latter approach as it proved to be computationally efficient. The LPT solver is limited to simulating low particle concentrations, while the Eulerian solver performs well across a wide range of conditions. A range of test cases available in the literature were used to validate the models, using both DNS and experimental data.

Results highlighted that segregated, equilibrium concentration profiles and deposited particle beds were formed over moderate timescales of 60–80 s after fully developed flow was established. Direct comparison of profiles for 0.03 vol% between Lagrangian and Eulerian methods showed high consistency, with small deviations in the near-wall region, most likely due to estimation of the maximum bed packing fraction in the Eulerian case. Using the Eulerian framework, it was found, most importantly, that the incorporation of a hindered settling model significantly reduced particle segregation at concentrations >3 vol%, in systems of different particle sizes. Understanding the level of particle segregation and deposition is critical to the transportation of suspensions in many multiphase flow environments, such as with nuclear wastes, where reducing pipeline blockages is imperative. In summary, the LES Eulerian-Eulerian hindered settling approach described and validated herein, provides a computationally efficient, yet high resolution methodology, that can be utilised to simulate high concentration particulate flows in pipes and clarifiers that are typical of many industrially relevant problems. Furthermore, the approach provides a platform for the incorporation of more complex dynamics associated with flocculated flows. Ongoing work is employing population balance equation techniques in OpenFOAM® to simulate flocculation build-up and shear breakdown in liquid–solid systems to extend current simulations beyond well-dispersed particles. Aggregate size changes over time will be coupled with the hindered settling model to simulate dynamic flocculation-controlled separation in both turbulent pipes and clarifier channel flows.

CRediT authorship contribution statement

Md Mahidul Haque Prodhan: Writing – original draft, Software, Methodology, Funding acquisition, Formal analysis, Data curation. **Michael Fairweather:** Supervision, Software, Project administration, Methodology. **Jeffrey Peakall:** Writing – review & editing, Supervision, Resources, Formal analysis. **Timothy N. Hunter:** Writing – review & editing, Supervision, Resources, Project administration, Funding acquisition, Conceptualization.

Declaration of competing interest

The authors declare the following financial interests/personal relationships which may be considered as potential competing interests: Md Mahidul Haque Prodhan reports financial support was provided by Bangabandhu Overseas Scholarship Authority. The other authors declare that they have no known competing financial interests or personal relationships that could have appeared to influence the work reported in this paper.

Acknowledgements

Md M. H. Prodhan acknowledges the Bangabandhu Overseas Scholarship Authority of the University of Dhaka, Bangladesh for PhD funding. Thanks are also given to Research Computing at the University of Leeds for providing access to the ARC 3 and ARC 4 computing platforms. Lastly, thanks are given to the editor and anonymous reviewers, for their insightful comments that helped improve the final manuscript.

Appendix A. Supplementary data

Supplementary data to this article can be found online at https://doi.org/10.1016/j.ces.2026.124502.

Data availability

Data will be made available on request.

References

Abam, F.I., Dilibe, N.I., Nwankwojike, B.N., Diemuodeke, O., John, I., 2021. Comparative evaluation of homogenous and drift-flux models for a three-phase downward flow in a pipe. Sci. Afr. 13, e00898. https://doi.org/10.1016/j.sciaf.2021.e00898.

Ahmed, S., Mohanty, S., 2018. Numerical analysis of slurry flow characteristics through horizontal pipeline using CFD. Int. J. Eng. Technol. 5, 1348–1354.

Antonopoulou, E., Rohmann-Shaw, C.F., Sykes, T.C., Cayre, O.J., Hunter, T.N., Jimack, P.K., 2018. Numerical and experimental analysis of the sedimentation of spherical colloidal suspensions under centrifugal force. Phys. Fluids 30, 030702. https://doi.org/10.1063/1.5010735.

Arolla, S.K., Desjardins, O., 2015. Transport modeling of sedimenting particles in a turbulent pipe flow using Euler–Lagrange large eddy simulation. Int. J. Multiph. Flow 75, 1–11. https://doi.org/10.1016/j.ijmultiphaseflow.2015.04.010.

Bagchi, P., Balachandar, S., 2003. Effect of turbulence on the drag and lift of a particle. Phys. Fluids 15, 3496–3513. https://doi.org/10.1063/1.1616031.

Bajpai, A., Wangikar, A.U., Tewari, C., Kumar, R., 2025. Computational investigation of moving shock interaction with a granular particle curtain using a coupled Eulerian–Lagrangian approach. Phys. Fluids 37, 013374. https://doi.org/10.1063/5.0244485.

Baker, M.C., Kong, B., Capecelatro, J., Desjardins, O., Fox, R.O., 2020. Direct comparison of Eulerian–Eulerian and Eulerian–Lagrangian simulations for particle-laden vertical channel flow. AIChE J 66, e16230. https://doi.org/10.1002/aic.16230.

Benn, F.A., Fawell, P.D., Halewood, J., Austin, P.J., Costine, A.D., Jones, W.G., Francis, N.S., Druett, D.C., Lester, D., 2018. Sedimentation and consolidation of different density aggregates formed by polymer-bridging flocculation. Chem. Eng. Sci. 184, 111–125. https://doi.org/10.1016/j.ces.2018.03.037.

Borée, J., Caraman, N., 2005. Dilute bidispersed tube flow: Role of interclass collisions at increased loadings. Phys. Fluids 17, 055108. https://doi.org/10.1063/1.1897636.

Boutsikakis, A., Fede, P., Pedrono, A., Simonin, O., 2020. Numerical simulations of short- and long-range interaction forces in turbulent particle-laden gas flows. Flow Turbul. Combust. 105, 989–1015. https://doi.org/10.1007/s10494-020-00115-3.

Capecelatro, J., Desjardins, O., 2013. Eulerian–Lagrangian modeling of turbulent liquid–solid slurries in horizontal pipes. Int. J. Multiph. Flow 55, 64–79. https://doi.org/10.1016/j.ijmultiphaseflow.2013.04.006.

Capecelatro, J., Desjardins, O., 2013. An Euler–Lagrange strategy for simulating particle-laden flows. J. Comput. Phys. 238, 1–31. https://doi.org/10.1016/j.jcp.2012.12.015.

Caraman, N., Borée, J., Simonin, O., 2003. Effect of collisions on the dispersed phase fluctuation in a dilute tube flow: Experimental and theoretical analysis. Phys. Fluids 15, 3602–3612. https://doi.org/10.1063/1.1619136.

Chen, X., Wang, S., Shao, B., Xie, L., Kuang, G., Ma, Y., 2024. Study on the anisotropic flow characteristics of wet particles in liquid-solid fluidized beds. Powder Technol. 441, 119821. https://doi.org/10.1016/j.powtec.2024.119821.

Chengxi, Y., Seungjae, L., Dongbin, H., Taesung, K., 2024. Numerical modelling on dispersion behavior of particulate contamination induced by a moving operator in a semiconductor cleanroom: a eulerian-eulerian method. J. Build. Eng. 96, 110409. https://doi.org/10.1016/j.jobe.2024.110409.

Costa, P., Brandt, L., Picano, F., 2020. Interface-resolved simulations of small inertial particles in turbulent channel flow. J. Fluid Mech. 883, A54. https://doi.org/10.1017/jfm.2019.918.

Cui, G., Emadzadeh, A., Ooi, A., Philip, J., 2025. Experimental study of inertial particles in a horizontal turbulent pipe flow: neutrally buoyant and denser-than-fluid particles. J. Fluid Mech. 1008, A2. https://doi.org/10.1017/jfm.2025.105.

Cui, G., Emadzadeh, A., Xu, Z., Monty, J., Philip, J., 2026. Experimental study of particle-laden turbulent horizontal pipe flows up to $Re\tau \approx$ 2000 in the two-way coupling regime. Int. J. Multiph. Flow 197, 105591. https://doi.org/10.1016/j.ijmultiphaseflow.2025.105591.

Cunliffe, C.J., Dodds, J.M., Dennis, D.J.C., 2021. Flow correlations and transport behaviour of turbulent slurries in partially filled pipes. Chem. Eng. Sci. 235, 116465. https://doi.org/10.1016/j.ces.2021.116465.

Dixit, S., Kumar, S., Pradhan, A.R., Kumar, S., Kumar, K., Vatin, N.I., Miroshnikova, T., Epifantsev, K., 2023. Numerical simulation of sand–water slurry flow through pipe bend using CFD. Int. J. Interact. Des. Manuf. Ijidem 17, 2373–2385. https://doi.org/10.1007/s12008-022-01004-x.

Duque-Daza, C.A., Ramirez-Pastran, J., Lain, S., 2021. Influence of particle mass fraction over the turbulent behaviour of an incompressible particle-laden flow. Fluids 6, 374. https://doi.org/10.3390/fluids6110374.

Dutta, P., Chattopadhyay, H., Nandi, N., 2022. Numerical studies on turbulent flow field in a 90 deg pipe bend. J. Fluids Eng. 144. https://doi.org/10.1115/1.4053547.

Ekambara, K., Sanders, R.S., Nandakumar, K., Masliyah, J.H., 2009. Hydrodynamic simulation of horizontal slurry pipeline flow using ANSYS-CFX. Ind. Eng. Chem. Res. 48, 8159–8171. https://doi.org/10.1021/ie801505z.

Elreafay, A.M., Salem, K.M., Abumandour, R.M., Dawood, A.S., Al Nuaimi, S., 2025. Effect of particle diameter and void fraction on gas–solid two-phase flow: a numerical investigation using the Eulerian–Eulerian approach. Comput. Part. Mech. 12, 289–311. https://doi.org/10.1007/s40571-024-00798-9.

Fazeli, M., Emdad, H., Mehdi Alishahi, M., Rezaeiravesh, S., 2024. Wall-modeled large eddy simulation of 90° bent pipe flows with/without particles: a comparative study. Int. J. Heat Fluid Flow 105, 109268. https://doi.org/10.1016/j.ijheatfluidflow.2023.109268.

Garg, H., Wang, L., Andersson, M., Fureby, C., 2024. Large eddy simulations of turbulent pipe flows at moderate Reynolds numbers. Phys. Fluids 36, 045138. https://doi.org/10.1063/5.0201967.

Germano, M., Piomelli, U., Moin, P., Cabot, W.H., 1991. A dynamic subgrid-scale eddy viscosity model. Phys. Fluids Fluid Dyn. 3, 1760–1765. https://doi.org/10.1063/1.857955.

Gillies, R.G., Shook, C.A., Xu, J., 2004. Modelling heterogeneous slurry flows at high velocities. Can. J. Chem. Eng. 82, 1060–1065. https://doi.org/10.1002/cjce.5450820523.

González-Lavín, G., García-Merino, B., Fernández-Maza, C., Bringas, E., Gómez-Coma, L., Fallanza, M., Ortiz, I., 2024. Tailored Euler-Lagrange modelling of microfluidic solid/liquid reactive separations. Chem. Eng. J. 495, 153393. https://doi.org/10.1016/j.cej.2024.153393.

Han, Z., Xu, Z., Sun, A., Yu, X., 2019. The deposition characteristics of micron particles in heat exchange pipelines. Appl. Therm. Eng. 158, 113732. https://doi.org/10.1016/j.applthermaleng.2019.113732.

He, Y., Gu, Z., Su, J., Chen, C., Zhang, M., Zhang, L., Lu, W., 2018. Coupling Eulerian-Lagrangian method of air-particle two-phase flow with population balance equations to simulate the evolution of vehicle exhaust plume. Int. J. Numer. Meth. Fluids 88, 117–140. https://doi.org/10.1002/fld.4514.

Heinrich, M., Schwarze, R., 2020. 3D-coupling of Volume-of-Fluid and Lagrangian particle tracking for spray atomization simulation in OpenFOAM. SoftwareX 11, 100483. https://doi.org/10.1016/j.softx.2020.100483.

Heng, J., New, T.H., Wilson, P.A., 2018. On the application of an Eulerian granular model towards dilute phase pneumatic conveying. Powder Technol. 327, 456–466. https://doi.org/10.1016/j.powtec.2017.12.069.

Hoque, M.A., Mallik, M.S.I., Hossain, M.S., Gope, R.C., Uddin, M.A., 2024. Large eddy simulation of a turbulent channel flow using dynamic Smagorinsky subgrid scale model and differential equation wall model. Int. J. Thermofluids 22, 100676. https://doi.org/10.1016/j.ijft.2024.100676.

Hunter, T.N., Peakall, J., Egarr, D., Cowell, D.M.J., Freear, S., Tonge, A.S., Horton, L., Rice, H.P., Smith, I., Malone, K., Burt, D., Barnes, M., Randall, G., Biggs, S., Fairweather, M., 2020. Concentration profiling of a horizontal sedimentation tank utilising a bespoke acoustic backscatter array and CFD simulations. Chem. Eng. Sci. 218, 115560. https://doi.org/10.1016/j.ces.2020.115560.

Hussain, S.T., Peakall, J., Barnes, M., Hunter, T., 2022. Simultaneous velocity and concentration profiling of nuclear waste suspensions in pipe-flow, using ultrasonic Doppler and backscatter analysis. Proc. Meet. Acoust. 45, 070002. https://doi.org/10.1121/2.0001525.

Jiang, X., Lai, C.-H., 2009. Numerical Techniques for Direct and Large-Eddy Simulations, CRC Press. Boca Raton. https://doi.org/10.1201/9781420075793.

Jo, Y.B., Park, S.-H., Yoo, H.S., Kim, E.S., 2022. GPU-based SPH-DEM method to examine the three-phase hydrodynamic interactions between multiphase flow and solid particles. Int. J. Multiph. Flow 153, 104125. https://doi.org/10.1016/j.ijmultiphaseflow.2022.104125.

Johnson, M., Peakall, J., Fairweather, M., Biggs, S., Harbottle, D., Hunter, T.N., 2016. Characterization of Multiple Hindered Settling Regimes in Aggregated Mineral Suspensions. Ind. Eng. Chem. Res. 55, 9983–9993. https://doi.org/10.1021/acs.iecr.6b02383.

Joshi, T., Parkash, O., Gallegos, R.K.B., Krishan, G., 2025. Comparative investigation of the energy consumption and heat transfer characteristics of Uni-modal and Bi-modal slurry flow through a straight pipe. Ocean Eng. 316, 119987. https://doi.org/10.1016/j.oceaneng.2024.119987.

Kaushal, D.R., Thinglas, T., Tomita, Y., Kuchii, S., Tsukamoto, H., 2012. CFD modeling for pipeline flow of fine particles at high concentration. Int. J. Multiph. Flow 43, 85–100. https://doi.org/10.1016/j.ijmultiphaseflow.2012.03.005.

Kaushal, D.R., Tomita, Y., 2007. Experimental investigation for near-wall lift of coarser particles in slurry pipeline using γ-ray densitometer. Powder Technol. 172, 177–187. https://doi.org/10.1016/j.powtec.2006.11.020.

Khalilitehrani, M., Abrahamsson, P.J., Rasmuson, A., 2014. Modeling dilute and dense granular flows in a high shear granulator. Powder Technol. 263, 45–49. https://doi.org/10.1016/j.powtec.2014.04.088.

Kramer, O.J.I., de Moel, P.J., Baars, E.T., van Vugt, W.H., Padding, J.T., van der Hoek, J.P., 2019. Improvement of the Richardson-Zaki liquid-solid fluidisation model on the basis of hydraulics. Powder Technol. 343, 465–478. https://doi.org/10.1016/j.powtec.2018.11.018.

Li, X., Yan, Y., Shang, Y., Tu, J., 2015. An Eulerian–Eulerian model for particulate matter transport in indoor spaces. Build. Environ. 86, 191–202. https://doi.org/10.1016/j.buildenv.2015.01.010.

Li, H., Zhang, Q., Zeng, M., Cao, J., Zhao, Q., Hao, L., 2023. Insights into gas flow behavior in venturi aerator by CFD-PBM model and verification of its efficiency in sludge reduction through O3 aeration. J. Water Process Eng. 54, 103960. https://doi.org/10.1016/j.jwpe.2023.103960.

Lilly, D.K., 1992. A proposed modification of the Germano subgrid-scale closure method. Phys. Fluids Fluid Dyn. 4, 633–635. https://doi.org/10.1063/1.858280.

Lockwood, A.P.G., Peakall, J., Warren, N.J., Randall, G., Barnes, M., Harbottle, D., Hunter, T.N., 2021. Structure and sedimentation characterisation of sheared Mg(OH) 2 suspensions flocculated with anionic polymers. Chem. Eng. Sci. 231, 116274. https://doi.org/10.1016/j.ces.2020.116274.

Lv, X.-F., Xu, K.-Y., Liu, Y., Wang, C.-S., Peng, M.-G., Du, H., Cao, S.-C., Ma, Q.-L., Zhou, S., Song, S.-F., 2024. Numerical simulation analysis of stable flow of hydrate slurry in gas-liquid-solid multiphase flow. Ocean Eng. 300, 117336. https://doi.org/10.1016/j.oceaneng.2024.117336.

Lysenko, D.A., Ertesvåg, I.S., Rian, K.E., 2013. Modeling of turbulent separated flows using OpenFOAM. Comput. Fluids 80, 408–422. https://doi.org/10.1016/j.compfluid.2012.01.015.

Marchioli, C., Bourgoin, M., Coletti, F., Fox, R., Magnaudet, J., Reeks, M., Simonin, O., Sommerfeld, M., Toschi, F., Wang, L.-P., Balachandar, S., 2025. Particle-laden flows. Int. J. Multiph. Flow 191, 105291. https://doi.org/10.1016/j.ijmultiphaseflow.2025.105291.

Messa, G.V., Yang, Q., Adedeji, O.E., Chára, Z., Duarte, C.A.R., Matoušek, V., Rasteiro, M.G., Sanders, R.S., Silva, R.C., de Souza, F.J., 2021. Computational fluid dynamics modelling of liquid–solid slurry flows in pipelines: state-of-the-art and future perspectives. Processes 9, 1566. https://doi.org/10.3390/pr9091566.

Ofei, T.N., Ismail, A.Y., 2016. Eulerian-Eulerian simulation of Particle-Liquid Slurry Flow in Horizontal Pipe. J. Pet. Eng. 2016, 5743471. https://doi.org/10.1155/2016/5743471.

Pal, R., 2019. Modeling of sedimentation and creaming in suspensions and pickering emulsions. Fluids 4, 186. https://doi.org/10.3390/fluids4040186.

Rashidi Gugheri, F., Pakravan, H.A., 2025. Numerical investigation and correlation development for pressure drop in pneumatic conveying through blinded T-bends. Powder Technol. 449, 120375. https://doi.org/10.1016/j.powtec.2024.120375.

Rice, H.P., Fairweather, M., Peakall, J., Hunter, T.N., Mahmoud, B., Biggs, S.R., 2015. Constraints on the functional form of the critical deposition velocity in solid–liquid pipe flow at low solid volume fractions. Chem. Eng. Sci. 126, 759–770. https://doi.org/10.1016/j.ces.2014.12.039.

Rice, H.P., Fairweather, M., Peakall, J., Hunter, T.N., Mahmoud, B., Biggs, S.R., 2015. Measurement of particle concentration in horizontal, multiphase pipe flow using acoustic methods: limiting concentration and the effect of attenuation. Chem. Eng. Sci. 126, 745–758. https://doi.org/10.1016/j.ces.2014.11.063.

Richardson, J.F., Zaki, W.N., 1997. Sedimentation and fluidisation: Part I. Chem. Eng. Res. Des. 75, S82–S100. https://doi.org/10.1016/S0263-8762(97)80006-8.

Roco, M.C., Shook, C.A., 1983. Modeling of slurry flow: the effect of particle size. Can. J. Chem. Eng. 61, 494–503. https://doi.org/10.1002/cjce.5450610402.

Sadeghi, M., Li, S., Zheng, E., Sontti, S.G., Esmaeili, P., Zhang, X., 2022. CFD simulation of Turbulent non-Newtonian Slurry Flows in Horizontal Pipelines. Ind. Eng. Chem. Res. 61, 5324–5339. https://doi.org/10.1021/acs.iecr.1c04471.

Saidi, M.S., Rismanian, M., Monjezi, M., Zendehbad, M., Fatehiboroujeni, S., 2014. Comparison between Lagrangian and Eulerian approaches in predicting motion of micron-sized particles in laminar flows. Atmos. Environ. 89, 199–206. https://doi.org/10.1016/j.atmosenv.2014.01.069.

Savari, C., Barigou, M., 2024. Multiscale analysis of turbulence in horizontal pipes: liquid and particle-liquid flow investigation. Phys. Fluids 36, 033311. https://doi.org/10.1063/5.0193241.

Schmitt, F.G., 2007. About Boussinesq's turbulent viscosity hypothesis: historical remarks and a direct evaluation of its validity. Comptes Rendus Mécanique 335, 617–627. https://doi.org/10.1016/j.crme.2007.08.004.

Shajahan, T., Schouten, T., Raaghav, S.K.R., van Rhee, C., Keetels, G., Breugem, W.-P., 2024. Characteristics of slurry transport regimes: Insights from experiments and interface-resolved Direct Numerical Simulations. Int. J. Multiph. Flow 176, 104831. https://doi.org/10.1016/j.ijmultiphaseflow.2024.104831.

Sharif Ahmadian, A., 2016. Chapter 5 - mathematical modeling and algorithm development. In: Sharif Ahmadian, A. (Ed.), Numer. Models Submerg. Break. Butterworth-Heinemann, Boston, pp. 77–92 https://doi.org/10.1016/B978-0-12-802413-3.00005-5.

Tanguay, M., Fawell, P., Adkins, S., 2014. Modelling the impact of two different flocculants on the performance of a thickener feedwell. App. Math. Model. 38, 4262–4276. https://doi.org/10.1016/j.apm.2014.04.047.

Tian, R., Wang, S., Li, X., Yuan, Z., Shao, B., Fan, J., 2021. Hydrodynamics of wet particles in liquid-solid fluidized beds using kinetic theory of rough spheres model. Powder Technol. 392, 524–535. https://doi.org/10.1016/j.powtec.2021.07.029.

Turney, D.E., Kalaga, D.V., Ansari, M., Yakobov, R., Joshi, J.B., 2018. Reform of the drift-flux model of multiphase flow in pipes, wellbores, and reactor vessels. Chem. Eng. Sci. 184, 251–258. https://doi.org/10.1016/j.ces.2018.03.033.

Vakilzadeh, A., Bagheri Sarvestani, A., Osloob, R., Kamali, R., 2023. Sensitivity analysis of kinetic theory of granular flow (KTGF) and mixture models in terms of involved elemental parameters for two-phase gas-solid flow. Part. Sci. Technol. 41, 1156–1169. https://doi.org/10.1080/02726351.2023.2186990.

Vegendla, S.N.P., Heynderickx, G.J., Marin, G.B., 2011. Comparison of Eulerian–Lagrangian and Eulerian–Eulerian method for dilute gas–solid flow with side inlet. Comput. Chem. Eng. 35, 1192–1199. https://doi.org/10.1016/j.compchemeng.2010.09.001.

Vijiapurapu, S., Cui, J., 2007. Simulation of turbulent flow in a ribbed pipe using Large Eddy simulation. Numer. Heat Transf. Part Appl. 51, 1137–1165. https://doi.org/10.1080/10407780601112829.

Vreman, A.W., 2007. Turbulence characteristics of particle-laden pipe flow. J. Fluid Mech. 584, 235–279. https://doi.org/10.1017/S0022112007006556.

Vreman, B., Geurts, B.J., Deen, N.G., Kuipers, J.A.M., Kuerten, J.G.M., 2009. Two- and four-way coupled Euler–Lagrangian Large-Eddy simulation of turbulent particle-laden channel flow. Flow Turbul. Combust. 82, 47–71. https://doi.org/10.1007/s10494-008-9173-z.

Wang, J., Lyu, Y., Jia, R., Wang, S., Ma, Z., 2025. Numerical investigation on flow characteristics of solid-liquid slurry within multi-sized particles through a horizontal pipe. Int. Commun. Heat Mass Transf. 163, 108731. https://doi.org/10.1016/j.icheatmasstransfer.2025.108731.

Wang, Y., Zhao, Y., Yao, J., 2019. Particle dispersion in turbulent, square open duct flows of high Reynolds number. Powder Technol. 354, 92–107. https://doi.org/10.1016/j.powtec.2019.05.085.

Wang, Y., Sun, J., Zhao, M., Murga, A., Yoo, S.-J., Ito, K., Long, Z., 2023. Numerical study of indoor oil mist particle concentration distribution in an industrial factory using the Eulerian–Eulerian and Eulerian–Lagrangian methods. Fluids 8, 264. https://doi.org/10.3390/fluids8100264.

Weller, H.G., Tabor, G., Jasak, H., Fureby, C., 1998. A tensorial approach to computational continuum mechanics using object-oriented techniques. Comput. Phys. 12, 620–631. https://doi.org/10.1063/1.168744.

Wolde, B., Mortimer, L.F., Fairweather, M., 2023. Stokes number effects on deposition in particle-laden turbulent pipe flows. Chem. Eng. Technol. 46, 1351–1361. https://doi.org/10.1002/ceat.202200606.

Wu, M., Zhang, J., Gui, N., Zou, Q., Yang, X., Tu, J., Jiang, S., Liu, Z., 2024. Advances in the modeling of multiphase flows and their application in nuclear engineering—A review. Exp. Comput. Multiph. Flow 6, 287–352. https://doi.org/10.1007/s42757-024-0202-5.

Yan, Q., Li, D., Wang, K., Zheng, G., 2024. Study on the hydrodynamic evolution mechanism and drift flow patterns of pipeline gas–liquid flow. Processes 12, 695. https://doi.org/10.3390/pr12040695.

Yang, X., Gupta, S., Kuo, T.-W., Gopalakrishnan, V., 2014. RANS and Large Eddy simulation of internal combustion engine flows—a comparative study. J. Eng. Gas Turbines Power 136. https://doi.org/10.1115/1.4026165.

Yang, Z., Savari, C., Barigou, M., 2022. Numerical and Experimental Investigations of Horizontal Turbulent Particle–Liquid Pipe Flow. Ind. Eng. Chem. Res. 61, 12040–12051. https://doi.org/10.1021/acs.iecr.2c02183.

Yao, R., Wang, Z., Huang, X., 2023. Design parameters investigation on sand transportation characteristics of V-inclined Pipe based on Eulerian–Eulerian two-phase flow model. Water 15, 4266. https://doi.org/10.3390/w15244266.

Zahtila, T., Chan, L., Ooi, A., Philip, J., 2023. Particle transport in a turbulent pipe flow: direct numerical simulations, phenomenological modelling and physical mechanisms. J. Fluid Mech. 957, A1. https://doi.org/10.1017/jfm.2022.987.

Zhang, Z., Chen, Q., 2007. Comparison of the Eulerian and Lagrangian methods for predicting particle transport in enclosed spaces. Atmos. Environ. 41, 5236–5248. https://doi.org/10.1016/j.atmosenv.2006.05.086.

Zhang, M., Kang, Y., Wei, W., Li, D., Xiong, T., 2021. CFD investigation of the flow characteristics of liquid–solid slurry in a large-diameter horizontal pipe. Part. Sci. Technol. 39, 712–725. https://doi.org/10.1080/02726351.2020.1799274.

Zhang, X., Liu, C., Liao, W., Wang, S., Zhang, W., Xie, J., Gao, Z., 2022. Separation efficiency of different solid-liquid separation technologies for slurry and gas emissions of liquid and solid fractions: a meta-analysis. J. Environ. Manage. 310, 114777. https://doi.org/10.1016/j.jenvman.2022.114777.

Zhang, L., Wang, H., Wu, A., Yang, K., Zhang, X., Guo, J., 2023. Effect of flocculant dosage on the settling properties and underflow concentration of thickener for flocculated tailing suspensions. Water Sci. Technol. 88, 304–320. https://doi.org/10.2166/wst.2023.191.

Zhang, X., Yin, Z., Wang, Y., Yang, B., Zheng, F., 2024. Analysis of the correlation between vegetated flow and suspended sediment using the drift flux model. Phys. Fluids 36, 043318. https://doi.org/10.1063/5.0198118.

Zhao, B., Yang, C., Yang, X., Liu, S., 2008. Particle dispersion and deposition in ventilated rooms: Testing and evaluation of different Eulerian and Lagrangian models. Build. Environ. 43, 388–397. https://doi.org/10.1016/j.buildenv.2007.01.005.

Zhao, R., Zhang, Y., Zhang, X., Wang, X., 2024. Validation of a Eulerian–Lagrangian numerical algorithm for simulating ultra-coarse particles transported in horizontal and vertical hydraulic pipes. Comput. Fluids 276, 106263. https://doi.org/10.1016/j.compfluid.2024.106263.

Zheng, E., Rudman, M., Kuang, S., Chryss, A., 2020. Turbulent coarse-particle suspension flow: Measurement and modelling. Powder Technol. 373, 647–659. https://doi.org/10.1016/j.powtec.2020.06.080.